U.S. GEOLOGICAL SURVEY SUBSIDENCE INTEREST GROUP CONFERENCE, PROCEEDINGS OF THE TECHNICAL MEETING, LAS VEGAS, NEVADA, FEBRUARY 14–16,1995

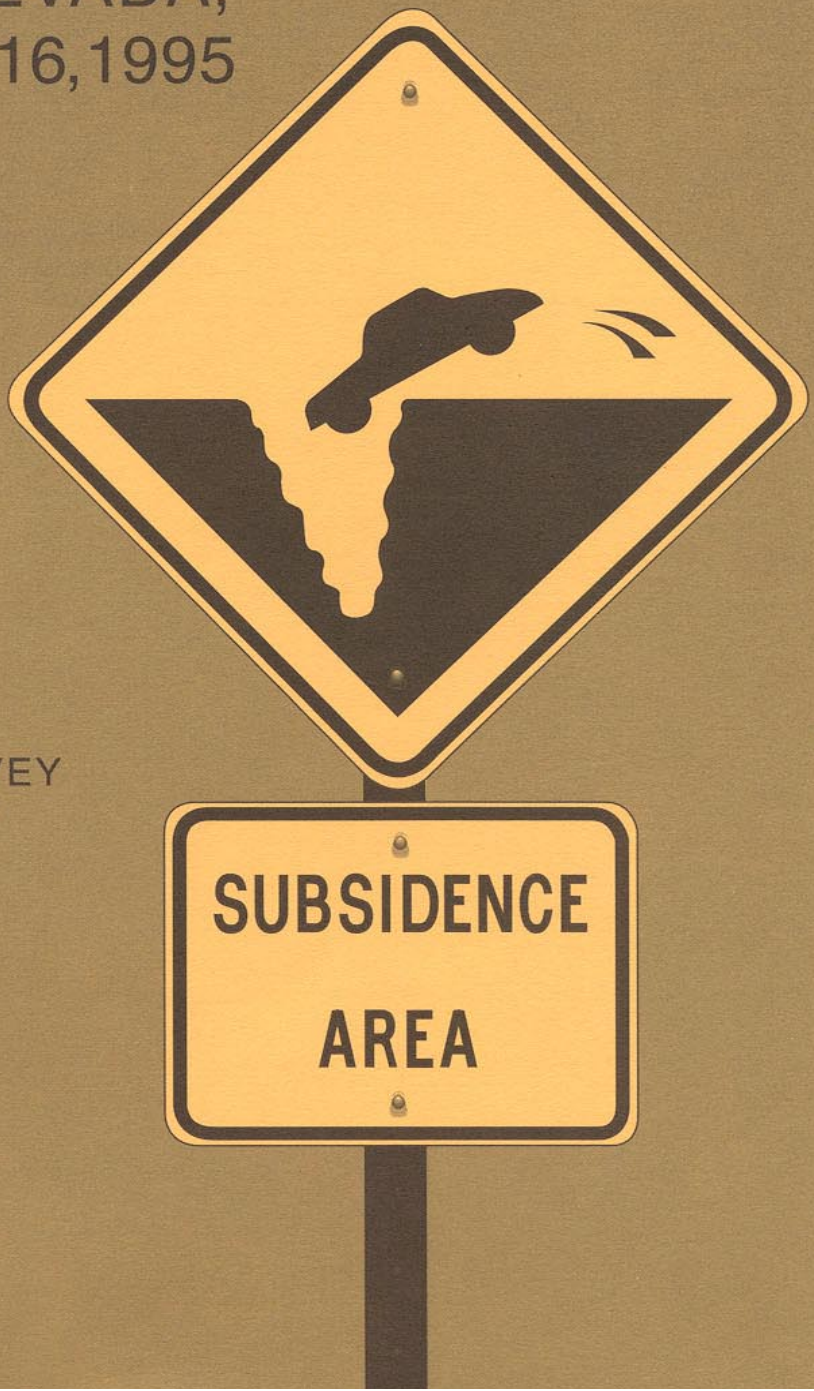

U.S. GEOLOGICAL SURVEY
Open-File Report 97—47

U.S. DEPARTMENT OF THE INTERIOR
MARCH 3, 1849

Report Documentation Page

Form Approved
OMB No. 0704-0188

1. REPORT DATE	2. REPORT TYPE	3. DATES COVERED
1997	**N/A**	**-**

4. TITLE AND SUBTITLE	5a. CONTRACT NUMBER
U.S. Geological Survey Subsidence Interest Group Conference, Proceedings of the Technical Meeting, Las Vegas, Nevada, February 14-16, 1995	5b. GRANT NUMBER
	5c. PROGRAM ELEMENT NUMBER
6. AUTHOR(S)	5d. PROJECT NUMBER
	5e. TASK NUMBER
	5f. WORK UNIT NUMBER
7. PERFORMING ORGANIZATION NAME(S) AND ADDRESS(ES) **U.S. Department of the Interior 1849 C Street, NW Washington, DC 20240**	8. PERFORMING ORGANIZATION REPORT NUMBER
9. SPONSORING/MONITORING AGENCY NAME(S) AND ADDRESS(ES)	10. SPONSOR/MONITOR'S ACRONYM(S)
	11. SPONSOR/MONITOR'S REPORT NUMBER(S)

12. DISTRIBUTION/AVAILABILITY STATEMENT
Approved for public release, distribution unlimited

13. SUPPLEMENTARY NOTES
The original document contains color images.

14. ABSTRACT

15. SUBJECT TERMS

16. SECURITY CLASSIFICATION OF:			17. LIMITATION OF ABSTRACT	18. NUMBER OF PAGES	19a. NAME OF RESPONSIBLE PERSON
a. REPORT	b. ABSTRACT	c. THIS PAGE			
unclassified	**unclassified**	**unclassified**	**SAR**	**42**	

Cover: Sign warning motorists of subsidence hazard was erected after an earth fissure damaged Snyder Hill Road in Pima County, Arizona, 1981.

U.S. Geological Survey Subsidence Interest Group Conference, Proceedings of the Technical Meeting, Las Vegas, Nevada, February 14–16, 1995

By Keith R. Prince and S.A. Leake, Editors

U.S. GEOLOGICAL SURVEY
Open-File Report 97–47

Tucson, Arizona
1997

U.S. DEPARTMENT OF THE INTERIOR
BRUCE BABBITT, Secretary

U.S. GEOLOGICAL SURVEY
Gordon P. Eaton, Director

For additional information
write to:

Regional Hydrologist
U.S. Geological Survey
345 Middlefield Road
Menlo Park, CA 94025-3591

Copies of this report can be
purchased from:

U.S. Geological Survey
Branch of Information Services
Box 25286
Denver, CO 80225-0286

CONTENTS

CONVERSION FACTORS

Multiply	By	To obtain
millimeter (mm)	0.03937	inch
centimeter (cm)	0.3937	inch
meter (m)	3.281	foot
kilometer (km)	0.6214	mile
kilogram (kg)	2.205	pound
hectare (ha)	2.471	acre
cubic meter per second (m^3/s)	35.3107	cubic foot per second
microradian per year (μrad/yr)	$5.73x10^{-5}$	degrees per year
liter per second (L/s)	0.2642	gallon per minute
per meter (m^{-1})	0.3048	per foot
Newton per meter (N/m)	0.06852	pounds per foot
Newton per square meter (N/m^2)	0.020885	pounds per square foot
Newton per cubic meter (N/m^3)	0.0063659	pounds per cubic foot
Pascal (Pa)	0.0001450	pounds per square inch
per Pascal (Pa^{-1})	689.5	per square inch per pound

In this report, temperature is reported in degrees Celsius (°C), which can be converted to degrees Fahrenheit (°F) by using the following equation:

$$°F = 1.8(°C) + 32$$

VERTICAL DATUM

Sea level: In this report, “sea level” refers to the National Geodetic Vertical Datum of 1929—A geodetic datum derived from a general adjustment of the first-order level nets of the United States and Canada, formerly called Sea Level Datum of 1929.

U.S. Geological Survey Subsidence Interest Group Conference, Proceedings of the Technical Meeting, Las Vegas, Nevada, February 14–16, 1995

HISTORY OF THE SUBSIDENCE INTEREST GROUP

By Keith R. Prince

Land subsidence is the loss of surface elevation as a result of the removal of subsurface support. The mechanisms by which this can occur may be natural in origin or induced by human activities. Common causes of land subsidence include the removal of oil, gas, and water from underground reservoirs; dissolution of limestone aquifers (sinkholes); underground mining activities; drainage of organic soils; and hydrocompaction (the initial wetting of dry soils). Overdraft of aquifers is the major cause of areally extensive land subsidence, and as ground-water pumping increases, land subsidence also will increase.

The U.S. Geological Survey (USGS) has a long-standing history of describing, mapping, and conducting process-oriented research in land subsidence. In 1955, the Geological Survey formed the "Mechanics of Aquifers Project" under the direction of Joseph F. Poland to study the processes that result in land subsidence due to the withdrawal of ground water. From 1955 to 1984, this research team gained international renown as they advanced the understanding of aquifer mechanics and land-subsidence theory. In addition to conducting pioneering research, this group also provided a focal point within the USGS for the dissemination of technology and scientific understanding in aquifer mechanics. In 1984, however, the "Mechanics of Aquifers Project" was terminated leaving no focal point for technology transfer in the USGS.

The USGS has continued to participate in a broad spectrum of cooperative and Federally funded projects in aquifer mechanics and land subsidence. These projects are designed to identify and monitor areas with the potential for land subsidence, conduct basic research in the processes that control land subsidence and the development of earth fissures, and develop new quantitative tools to predict aquifer-system deformation. In 1989, the "Aquifer Mechanics and Subsidence Interest Group" (referred to herein as the "Subsidence Interest Group") was formed to facilitate technology transfer and to provide a forum for the exchange of information and ideas among scientists actively working in subsidence and aquifer-mechanics projects. To stimulate technical interaction among the member scientists, periodic technical meetings are held in which the latest advances in monitoring and research are presented.

Introduction to Papers

This report is a compilation of short papers that are based on oral presentations summarizing the results of recent research that were given at the third meeting of the Subsidence Interest Group held in Las Vegas,

Nevada, February 14–16, 1995. The report includes case studies of land subsidence and aquifer-system deformation resulting from fluid withdrawal, geothermal development, and mine collapse. Methods for monitoring land subsidence using Global Positioning System technology for the rapid and accurate measurement of changes in land-surface altitude also are described. The current status of numerical simulation of land subsidence in the USGS is summarized, and several of the short papers deal with the development and application of new numerical techniques for simulation and quantification of aquifer-system deformation.

Not all oral presentations made at the meeting are documented in this report. Several of the presentations were of ongoing research and as such, the findings were provisional in nature and were offered at the meeting to stimulate scientific discussion and debate among colleagues. The information presented in this report, although only a subset of the proceedings of the meeting in Las Vegas, should help expand the scientific basis for management decisions to mitigate or control the effects of land subsidence. The short papers describing the results of these studies provide a cross section of ongoing research in aquifer mechanics and land subsidence and also form an assessment of the current technology and "state of the science." The analytical and interpretive methods described in this report will be useful to scientists involved in studies of ground-water hydraulics and aquifer-system deformation.

SUBSIDENCE INTEREST GROUP CONFERENCE AGENDA

Las Vegas, Nevada
February 14–16, 1995

Time	Subject	Presenters
	Tuesday, February 14, 1995	
8:00 a.m.	Welcome, Opening Comments	Keith Prince, Menlo Park, Calif.
	Session 1—Theoretical, Numerical, and Field Developments	
8:10	Numerical simulation of two-dimensional aquifer deformation—A finite-element model based on Biot theory	Paul Hsieh, Menlo Park, Calif.
8:50	Simulation of deformation of sediments from decline of ground-water levels in an aquifer underlain by a bedrock step	Stan Leake, Tucson, Ariz.
9:30	The state of subsidence modeling	Tom Burbey, Carson City, Nev.
10:10	Break	
10:30	Comments on poroviscosity	Don Helm, Reno, Nev.
11:10	Development and results of tilt sensors used in the study of beach deformation in the Grand Canyon	Mike Carpenter, Tucson, Ariz.
11:50	Lunch	
	Session 2—Measurement of Subsidence	
1:00 p.m.	Land-surface elevation changes associated with well-injection tests, Los Angeles County, California	Devin Galloway, Sacramento, Calif.; Don Pool, Tucson, Ariz.
1:40	Changes in subsidence patterns at Roger Lake, Edwards Air Force Base, California	James Blodgett, Sacramento, Calif.
2:20	Measurement and correlation of earth-fissure formation rates with hydrogeology, subsidence, and ground-water withdrawals in the Picacho Basin, central Arizona	Don Pool, Tucson, Ariz; Steve Slaff, Tucson, Ariz; and Phil Pearthree, Tucson, Ariz.
3:00	Break	
3:20	Deformation measurements in the Albuquerque Basin of New Mexico	Chuck Heywood, Albuquerque, N. Mex.
4:00	Results of Global Positioning System surveys in Antelope Valley, California	Marti Ikehara, Sacramento, Calif.
4:30	IBEX—An endangered species? The design of an incremental borehole extensometer probe	Francis Riley, Menlo Park, Calif.
4:45	Adjourn	
7:30	USGS Subsidence Interest Group Business Meeting	
	Wednesday, February 15, 1995 **Session 3—Subsidence Effects and Features**	
8:00 a.m.	Land subsidence at Luke Air Force Base, Arizona	Herb Schumann, Tempe, Ariz.
8:40	Deformation in the Casa Diablo and geothermal well field, eastern California	Chris Farrar, Carnelian Bay, Calif.; Jim Howle, Carnelian Bay, Calif.
9:20	Break	
9:40	Partial collapse of the Retsof Salt Mine, New York	Dorothy Tepper, Ithaca, N.Y.
10:20	Sinkhole development in the San Xavier District, Tucson, Arizona	Don Pool, Tucson, Ariz.
11:00	Lunch	
12:00 p.m.	Field Trip 1—Las Vegas Wash	Gary Dixon, Las Vegas, Nev.; John Whitney, Yucca Mountain Project, Denver, Colo.; and Pat Glancy, Carson City, Nev.
	Thursday, February 16, 1995	
8:00 a.m.	Field Trip 2—Subsidence in Las Vegas Valley	Don Helm, Reno, Nev.; Tom Burbey, Carson City, Nev.
12:00 p.m.	Adjourn	

This page intentionally left blank

Poroelasticity Simulation of Ground-Water Flow and Subsurface Deformation

By Paul A. Hsieh

INTRODUCTION

Withdrawal of ground water causes horizontal and vertical displacements in the subsurface. If the subsurface material is assumed to be linearly elastic, then poroelasticity theory, originally developed by Biot (1941), can be used to analyze the coupled interaction between ground-water flow and subsurface (matrix) deformation. In this study, a finite-element model is developed to solve the axisymmetric form of the poroelasticity equations. The model is used to analyze deformation-induced changes in hydraulic head, a phenomenon also known as the Noordbergum effect or reverse water-level fluctuation.

POROELASTICITY MODEL

In poroelasticity theory, fluid flow is described by Darcy's Law and mass conservation, and matrix deformation is described by Biot's constitutive relations and stress equilibrium. Strains are assumed to be small. In this study, it is further assumed that (a) the subsurface is in an initial state of hydraulic and mechanical equilibrium, (b) gravitational body force remains constant, (c) the matrix grains are incompressible, and (d) the fluid is compressible. Under the above assumptions, the equations of poroelasticity are (Verruijt, 1969, p. 342):

$$\kappa \nabla^2 h = \frac{\partial}{\partial t}(\nabla \bullet \underline{u}) + \frac{\rho_f g n}{K_f}\frac{\partial h}{\partial t} , \qquad (1)$$

and

$$G\nabla^2 \underline{u} + \frac{G}{1-2\nu}\nabla(\nabla \bullet \underline{u}) - \rho_f g \nabla h = 0 , \qquad (2)$$

where h is change in hydraulic head from the initial head, $\underline{u}$ is displacement vector of the skeletal matrix, t is time, κ is hydraulic conductivity, n is porosity, $\rho_f g$ and K_f are the specific weight and bulk modulus of the fluid, respectively, and G and ν are the shear modulus and drained Poisson's ratio of the skeletal matrix, respectively. A numerical model has been developed to solve the axisymmetric form of equations (1) and (2) following the finite-element method of Smith and Griffiths (1988, chap. 9). In this formulation, material properties are assumed uniform within each element, but properties may vary from one element to the next. The model, therefore, may be applied to solve problems with a nonuniform distribution of properties.

SIMULATION OF DEFORMATION-INDUCED CHANGES IN HYDRAULIC HEAD

The poroelasticity model is applied to simulate deformation-induced changes in hydraulic head that often are observed in aquitards when water is pumped from an adjacent aquifer. A hypothetical setting consists of a 100-meter thick, laterally extensive aquifer that is confined above and below by aquitards (fig. 1). The upper aquitard is 100 m thick, and the lower aquitard extends to a great depth. The water table coincides with the land surface, which is the top of the upper aquitard. A well is screened over the entire thickness of the aquifer, and for simplicity, the well is assumed to be cased throughout both aquitards. Ground water is pumped at a constant rate of 5×10^{-2} m^3/s. The hydraulic and mechanical properties used in the simulation are shown in table 1. The aquifer

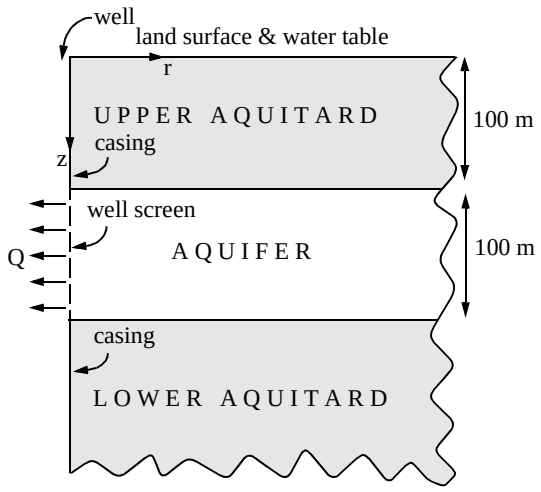

Figure 1. Hypothetical setting of an aquifer confined above and below by aquitards.

properties are characteristic of an unconsolidated, sandy formation. The two aquitards have identical properties that are characteristic of unconsolidated silty deposits.

In the numerical model, the aquifer and aquitards extend laterally from the well radius of 0.1 m to an outer boundary 10 km away. The outer boundary is impervious, and there is no change in stresses. The lower aquitard extends vertically to a bottom boundary 10 km below land surface. The bottom boundary is impervious, and there is no displacement. These two remote boundaries are sufficiently distant from the well screen so that slight variations in boundary conditions would not affect the solution in the region affected by pumping. The top boundary (land surface) is free of boundary traction, and drawdown of the water table is assumed negligible. At the well, there is no radial displacement and no change in the vertical component of boundary traction. This boundary condition allows the matrix along the well screen and (or) casing to move vertically but not horizontally. A uniform flux of water is withdrawn from the entire thickness of the aquifer so that no flow crosses the casing in the aquitards. The 10-kilometer by 10-kilometer model domain is discretized into a 40-column by 100-row mesh of rectangular elements with variable sizes. To prevent numerical oscillation, elements as thin as 0.1 m are used along aquifer-aquitard interfaces. The first time step is 15 seconds, and this time-step size is successively increased by 1.2 times until a total simulation time of 50 days is reached.

A 300- by 300-meter vertical section of aquifer and aquitards in their initial, undeformed states (before pumping) is shown in figure 2*A*. The well is on the left, land surface is at the top, and only the upper 100 m of the lower aquitard is shown. Horizontal and vertical grid lines, spaced 20 m apart, are superimposed on the section. By moving with the skeletal matrix, these grid lines illustrate the deformation of the aquifer and aquitards during pumping. Note that the grids shown in figure 2 are not the finite-element mesh used in the numerical model.

The simulated deformation of the aquifer and aquitards after 10 minutes of pumping is shown in figure 2*B*. For the sake of illustration, displacements are exaggerated 40,000 times so that, for example, a displacement of 40 m in figure 2*B* would correspond to an actual displacement of 1 mm. Contraction of the aquifer is evident. Horizontal contraction near the well is seen by the deflection of vertical grid lines towards the screen. A point initially at A in figure 2*A* has moved about 0.1 mm in the horizontal direction to A' in figure 2*B*. Vertical contraction can be seen by a

Table 1. Values of physical properties used in simulation

Physical property	Value in aquifer	Value in aquitards
Hydraulic conductivity, κ, in meters per second	1×10^{-4}	1×10^{-7}
Shear modulus, *G*, in Newton per square meter	3×10^{8}	3×10^{7}
Drained Poisson's ratio, ν (dimensionless).....	.25	.25
Porosity, *n* (dimensionless).....	.30	.40
Fluid bulk modulus, K_f, in Newton per square meter	2.3×10^{9}	2.3×10^{9}

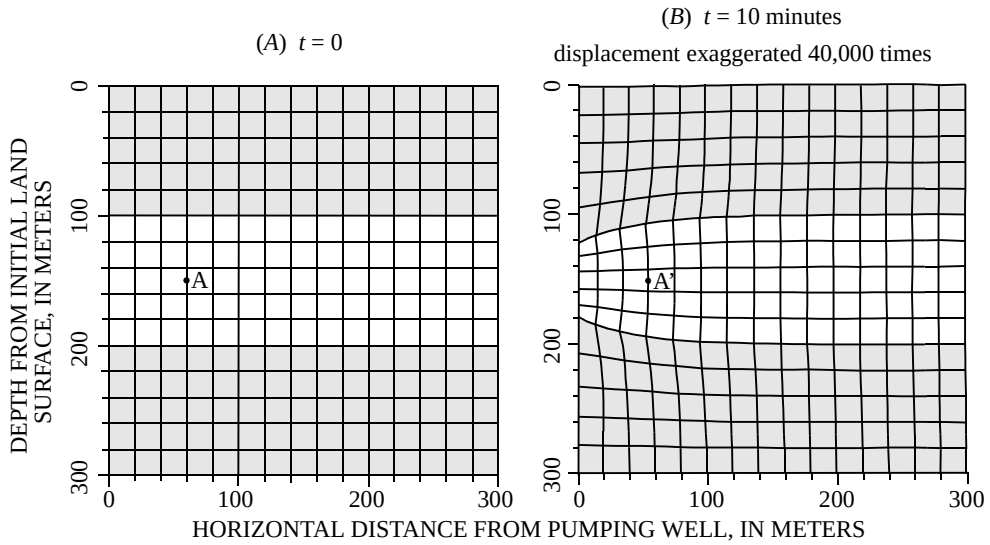

Figure 2. Deformation of a 300- by 300-meter vertical section of aquifer and aquitards with grid lines superimposed. Unshaded area indicates aquifer. Shaded area indicates aquitard. *t* is time since pumping began.

decrease of aquifer thickness. Immediately adjacent to the well, the decrease of thickness is about 1 mm, and the aquitards also have deformed. Near the well, the aquitards have contracted in the horizontal direction and extended in the vertical direction, and shear distortion increases toward the aquifer-aquitard interface.

The horizontal contraction and vertical extension in the aquitards cause local changes of pore volume. In some parts of the aquitard, pore volume increases, and in other parts, pore volume decreases. Understanding the relation between pore-volume change and head change is the key to understanding deformation-induced effects. During early time after the start of pumping, there is essentially no fluid flow in the aquitards. Under this condition, change in hydraulic head is inversely proportional to change in pore volume. At any point in the aquitard, if deformation results in a net increase in pore volume, hydraulic head drops. Conversely, if deformation results in a net decrease in pore volume, hydraulic head rises.

Progressive changes occur in hydraulic head in the 300- by 300-meter vertical section of aquifer and aquitards (fig. 3*A*–*F*). After 10 minutes of pumping (fig. 3*A*), two zones of induced head drop have developed—one above and one below the well screen. The head drops in both zones generally are between 0 and 1 cm. (The contour line for 1 cm of head drop lies close to the aquifer-aquitard interface). These two zones are regions of pore-volume increase in the aquitards. Two separate zones of induced head rise emerge in the upper aquitard. The shallower zone is just below land surface and near the well. The deeper zone occurs at the base of the aquitard and about 50 m radially outward from the well. The zones are the regions of pore-volume reduction in the aquitard.

As pumping continues, the aquifer contracts further and induces greater head changes in the aquitards. The maximum head rise exceeds 3 cm after 1 hour of pumping (fig. 3*B*), and 6 cm after 6 hours (fig. 3*C*). Head rise is greater in the upper aquitard than in the lower aquitard. The asymmetry is due to the presence of land surface where the absence of traction allows more deformation of the near-surface material. Of the two zones of head rise in the upper aquitard, the shallower one (just below land surface) has greatly expanded, and the deeper one has almost merged with the expanding contours. Of the two zones of head rise, the one above the well screen has almost disappeared, and the one below the well screen has remained about the same. These results show that, in the present case, head rise is the dominant effect induced by

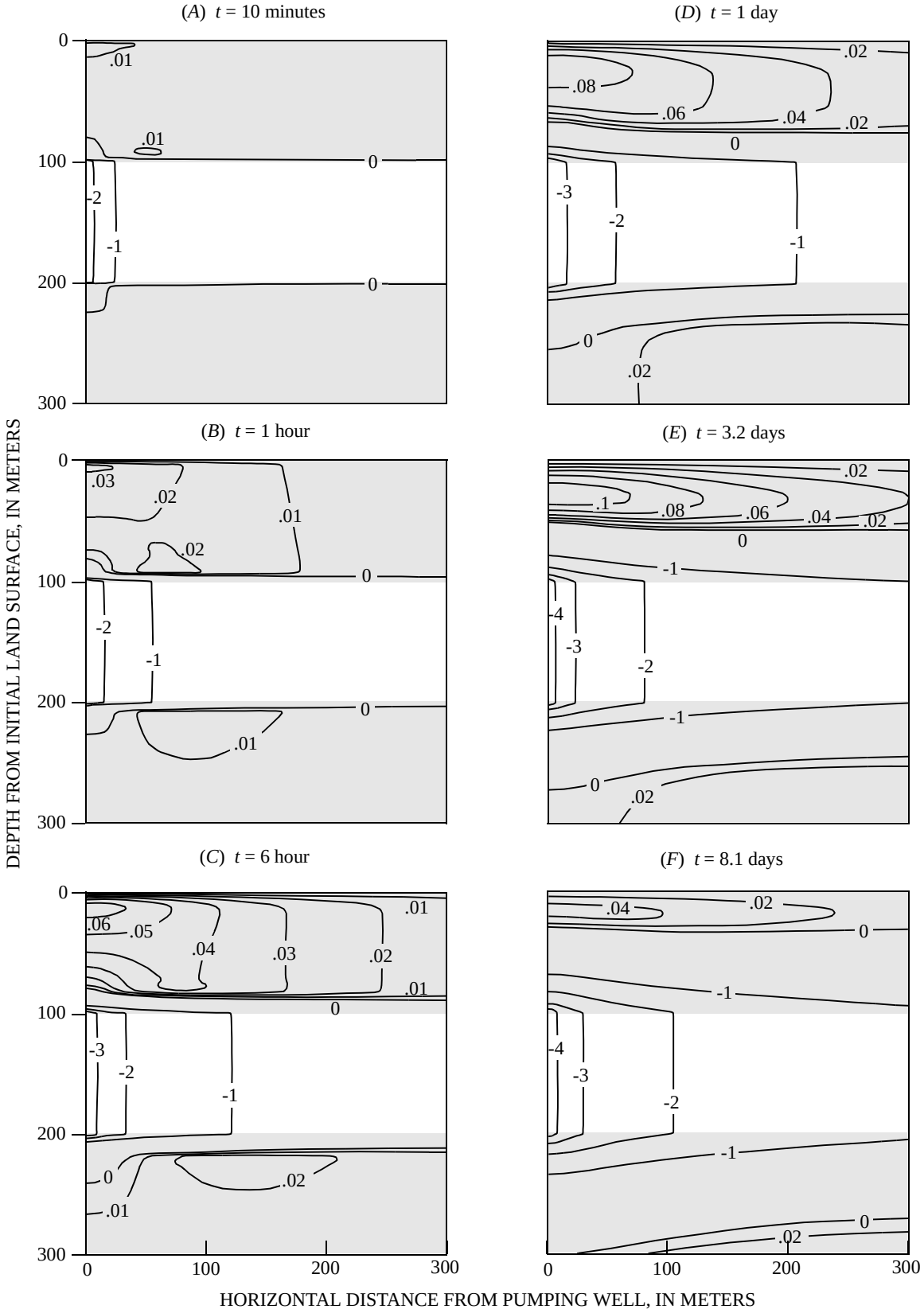

Figure 3. Changes in hydraulic head, in meters, in 300- by 300-meter vertical section of aquifer and aquitards. Unshaded area indicates aquifer. Shaded area indicates aquitard. Positive numbers indicate head rise, in meters. Negative numbers indicate head drop, in meters, Contour interval is irregular. *t* is time since pumping began.

pumping. Head drop is confined to a relatively small region above and below the well screen.

The deformation-induced head rise is dissipated over time by: (1) fluid flow from regions of higher head to regions of lower head (including the water table) and (2) propagation of head drop from the aquifer into the aquitards (fig. 3*D*, *E*, and *F*). After 1 day of pumping, head drop has propagated into the lower quarter of the upper aquitard. Above this zone of head drop, hydraulic head is still increasing (exceeding 8 cm), but flow to the water table has displaced the maximum to a lower position than before. After 3.2 days, the maximum head rise exceeds 10 cm; however, the region of head rise in the upper aquitard now encompasses only its upper half. By 8.1 days, the maximum head rise has decreased to about 4 cm, indicating significant dissipation of deformation-induced effects. After 14 days (not shown), head drop has propagated throughout the upper aquitard, and deformation-induced effects are no longer observable.

CONCLUSIONS

A simulation using a poroelasticity model with typical aquifer and aquitard properties shows that three-dimensional deformation caused by ground-water withdrawal from a confined or semiconfined aquifer can induce hydraulic-head changes in adjacent aquitards. The deformation-induced head changes range from about 1 cm of head drop to about 10 cm of head rise. These results are consistent with reported field observations. The simulation suggests that in a thick aquitard, induced head rise could persist for many days after the start of pumping but is eventually dissipated by (1) fluid flow from regions of higher head to regions of lower head and (2) propagation of drawdown from the pumped aquifer into the aquitard. The poroelasticity model developed for this analysis is useful in understanding the hydraulic response to ground-water withdrawal in layered aquifer-aquitard systems.

REFERENCES CITED

Biot, M.A., 1941, General theory of three-dimensional consolidation: Journal of Applied Physics, v. 12, p. 155–164.

Smith, I.M., and Griffiths, D.V., 1988, Programming the finite element method, 2nd ed.: Chinchester, John Wiley and Sons, 469 p.

Verruijt, A., 1969, Elastic storage of aquifers, *in* De Wiest, R.J.M., ed., Flow Through Porous Media: New York, Academic Press, p. 331–376.

Simulation of Deformation of Sediments from Decline of Ground-Water Levels in an Aquifer Underlain by a Bedrock Step

By S.A. Leake *and* Paul A. Hsieh

INTRODUCTION

Land subsidence occurs in many areas where ground-water pumping lowers water levels within compressible aquifer systems. In the southwestern United States, aquifer-system compaction and land subsidence have resulted in earth fissures—particularly along the margins of aquifers in alluvial basins that have extensive ground-water pumpage. One explanation for the development of fissures is horizontal extensional strain that could develop over buried bedrock highs or steps (Jachens and Holzer, 1982; Carpenter, 1993). Commonly applied methods of evaluating aquifer-system compaction (Leake and Prudic, 1991) are applications of the Terzaghi theory, in which all compaction is assumed to be vertical. Neglecting the horizontal components of deformation does not allow for complete analysis of problems of earth fissuring. Furthermore, the one-dimensional approach raises questions regarding the validity of computed distributions of head and vertical deformation in systems where horizontal deformation is significant. The more rigorous Biot (1941) theory of deformation accounts for horizontal as well as vertical components of elastic deformation. The purpose of this analysis is to evaluate relative importance of horizontal and vertical components of deformation in an aquifer underlain by a bedrock step.

APPROACH

Deformation around a bedrock step was simulated in a vertical plane for an idealized aquifer system (fig. 1). The right side of the plane is analogous to an edge of an alluvial basin, and the left side is analogous to an interior part of a basin where ground-water pumping causes water levels to decline. The aquifer system includes an upper unconfined compressible aquifer, a middle compressible confining unit, and a lower compressible confined aquifer.

Ground-water flow and deformation in the hypothetical system were simulated using two different methods. The first method used the MODFLOW finite-difference ground-water model program (McDonald and Harbaugh, 1988) to simulate ground-water flow in the vertical plane. Vertical compaction, Δb, is computed using the relation

$$\Delta b = -S_{sk} b \Delta h ,$$

where S_{sk} is the skeletal component of specific storage, b is thickness of compacting sediments, and Δh is change in head computed by MODFLOW. The relation is consistent with the Terzaghi theory (Leake and Prudic, 1991, equation 5). Compaction is computed for each cell, and vertical displacement is computed as half of the compaction for a cell plus the sum of compaction values for the cells below. The second method is a finite-element solution of flow and deformation in two dimensions. Fluid flow is described by Darcy's Law and mass conservation, and matrix deformation is described by Biot's constitutive relations and stress equilibrium. For more details on this method, see paper entitled "Poroelasticity Simulation of Ground-Water Flow and Subsurface Deformation" on page 5 in this report. In this paper, the two methods are referred to as the Terzaghi method and the Biot method, respectively.

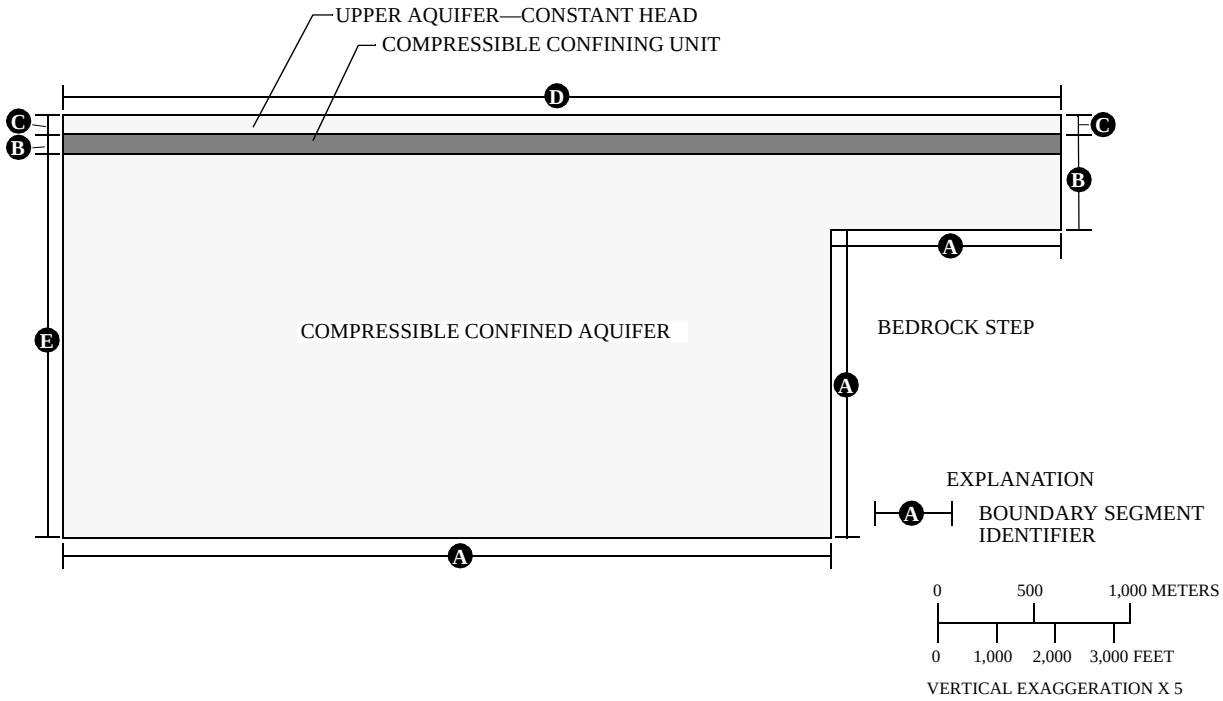

Figure 1. Hydrologic system used in simulations of flow and deformation.

For simplicity in simulating flow and deformation in vertical sections, the head in the upper aquifer was specified to remain constant for the entire period of simulation; therefore, no compaction occurs in that aquifer. The hydraulic boundary conditions (table 1) allow for a specified decline in head in the lower aquifer along the left side of the model. Along boundary-segment E (fig. 1), head is specified to linearly decline by 60 m over a 10-year period (fig. 2).

The Terzaghi method as applied for this analysis does not compute displacements along the edges of the model, but allows for vertical displacement at the centers of all model cells. The mechanical boundary conditions for the Biot method (table 1) allow for vertical displacement everywhere except along the lower boundary including the step. Horizontal displacement is allowed along the top boundary.

In the finite-difference and finite-element models, the hydrologic system is represented using 26 horizontal rows and 65 vertical columns of cells and elements. Rows are 20 m thick in the aquifers and 4 m thick in the confining unit, and each column is 80 m wide. The hydraulic and physical properties used in the simulations are given in table 2. The values are within ranges expected in alluvial basins in the southwestern United States (Hanson, 1989). Simulations with the Terzaghi method used a single skeletal specific-storage

Table 1. Boundary conditions used in simulations of flow and deformation

Boundary-segment identifier	Hydraulic boundary condition	Mechanical boundary condition used in Biot method
A	No flow	No horizontal or vertical displacement
B	No flow	No horizontal displacement
C	Specified head (constant)	No horizontal displacement
D	Specified head (constant)	Free surface
E	Specified head (declining)	No horizontal displacement

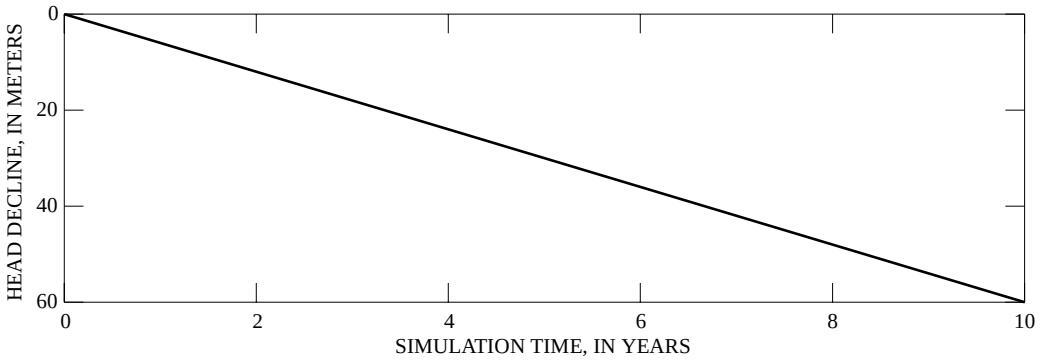

Figure 2. Specified decline in head along boundary-segment E.

Table 2. Hydraulic and physical properties used in simulations of flow and deformation

Hydrologic unit	Hydraulic conductivity (meter day^{-1})	Skeletal specific storage (meter^{-1})	Young's modulus (Newton meter^{-1})	Poisson's ratio
Upper aquifer	25	1×10^{-5}	8×10^{8}	0.25
Middle confining unit	.01	1×10^{-4}	8×10^{7}	.25
Lower aquifer.....	25	1×10^{-5}	8×10^{8}	.25

value rather than elastic and inelastic specific-storage values. The values of 1×10^{-5} m^{-1} for the aquifers and 1×10^{-4} m^{-1} for the confining unit are in the range of typical values for the skeletal component of inelastic specific storage. Using these values, this analysis is valid only for the case in which pore pressures do not increase (fig. 2). The Biot method does not use specific storage but rather uses Young's modulus and Poisson's ratio. The values given in table 2 are consistent with the specific-storage values used in the Terzaghi method. Although the Biot method is applicable to an elastic medium, the application here with properties corresponding to typical inelastic specific-storage values is appropriate as long as the Young's modulus and Poisson's ratio can be assumed to remain constant.

RESULTS

A comparison of results of the two methods can be used to evaluate the effects of ignoring horizontal deformation on computed head change. The results for the 10-year simulations using the Terzaghi and Biot methods are the same except at the extreme edge of the basin (fig. 3*A*); therefore, the assumptions inherent in the Terzaghi method have little effect on the computation of head change. Similarly, computed vertical displacement is almost identical over most of the area (fig. 3*B*). Within a distance of about one aquifer thickness on each side of the bedrock step, the distributions differ. The distribution computed by the Terzaghi method includes a discontinuity over the bedrock step. The displacement in the upper cell in the thin part of the aquifer adjacent to the step is less than 0.08 m, and the displacement in the upper cell in the thick part of the aquifer adjacent to the step is more than 0.18 m. The displacement in the upper cell in the thin part of the aquifer computed by the Biot method also is less than 0.08 m; however, the displacement computed by the Biot method in the upper cell in the thick part of the aquifer is only 0.10 m. Furthermore, the Biot method results in a smooth continuous distribution of displacement across the step.

The results of the Biot method can be useful for analysis of conditions leading to earth fissuring. The horizontal strain at land surface computed by the method (fig. 4) shows a tensional strain of more than 1×10^{-4} on the upside of the step. Although strain at failure is not well known, Jachens and

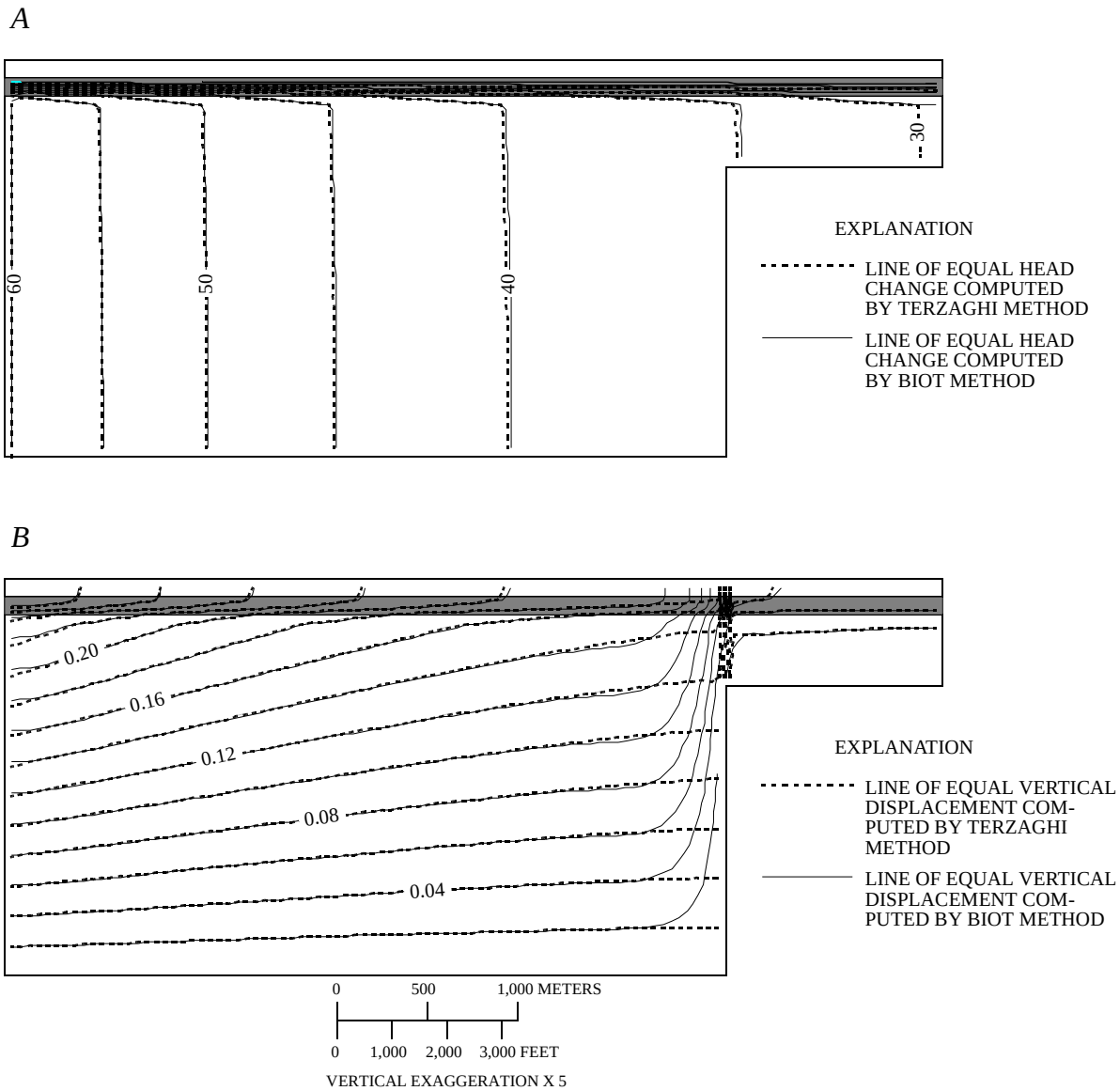

Figure 3. Results of simulations of flow and deformation using the Terzaghi and Biot methods. *A*, Computed head change, in meters. *B*, Computed vertical displacement, in meters.

Holzer (1982) calculate values in the range of 2×10^{-4} to 2×10^{-3}.

CONCLUSIONS

Head changes computed by the Terzaghi and Biot methods were almost identical throughout the simulated flow system. Vertical displacements computed by the two methods were almost the same except near the bedrock step. For the conditions simulated, the simpler Terzaghi method adequately describes deformation on a regional scale. For analysis of smaller-scale deformation around the bedrock step, the more rigorous Biot method is needed to adequately simulate vertical and horizontal deformation. The deformation computed by the Biot method can be used to calculate potential horizontal strains that lead to development of earth fissures.

REFERENCES

Biot, M.A., 1941, General theory of three-dimensional consolidation: Journal of Applied Physics, v. 12, p. 155–164.

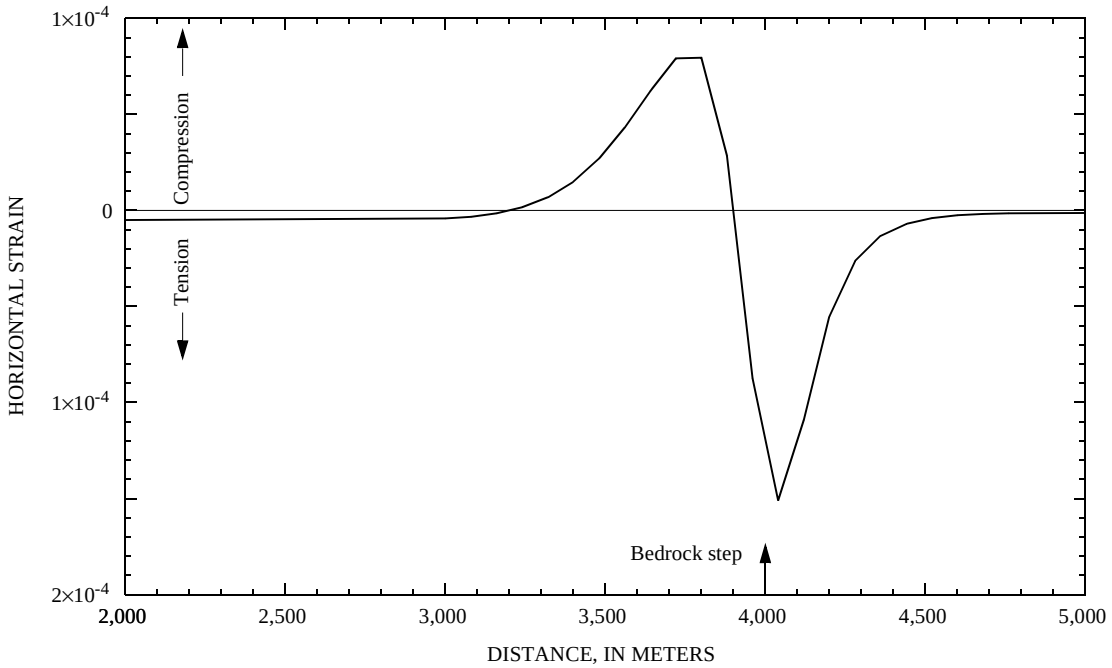

Figure 4. Horizontal strain at land surface at the end of the 10-year simulation computed by the Biot method.

Carpenter, M.C., 1993, Earth-fissure movements associated with fluctuations in ground-water levels near the Picacho Mountains, south-central Arizona: U.S. Geological Survey Professional Paper 497–H, 49 p.

Hanson, R.T., 1989, Aquifer-system compaction, Tucson basin and Avra Valley, Arizona: U.S. Geological Survey Water-Resources Investigations Report 88–4172, 69 p.

Jachens, R.C., and Holzer, T.L., 1982, Differential compaction mechanism for earth fissures near Casa Grande, Arizona: Geological Society of America Bulletin, v. 93, no. 10, p. 998–1012.

Leake, S.A., and Prudic, D.E., 1991, Documentation of a computer program to simulate aquifer-system compaction using the modular finite-difference ground-water flow model: U.S. Geological Survey Techniques of Water-Resources Investigations, book 6, chap. A2, 68 p.

McDonald, M.G., and Harbaugh, A.W., 1988, A modular three-dimensional finite-difference ground-water flow model: U.S. Geological Survey Techniques of Water-Resources Investigations, book 6, chap. A1, 586 p.

State of Subsidence Modeling Within the U.S. Geological Survey

By Thomas J. Burbey

Much of the current knowledge of land subsidence and aquifer deformation came from the U.S. Geological Survey's Mechanics of Aquifers Project led by Joseph F. Poland from 1955 through 1984. Until the advent of efficient and powerful computers, many of the calculations used to estimate vertical subsidence were done with analytical models (Poland and Davis, 1969). Beginning in the 1970's, Terzaghi's principle of effective stress coupled with Hubbert's force potential and Darcy's Law provided the basis for one-dimensional subsidence modeling (Gambolati and others, 1974; Helm, 1975, 1976). Helm's one-dimensional consolidation model was developed for constant and stress-dependent parameters, but was not linked to a ground-water flow model. Although Helm's model remains a powerful tool for detailed analysis of vertical effects at a specific site, it is not a model for basin-wide analysis. The first subsidence model incorporated into a ground-water flow model was written by Meyer and Carr (1979). This model allowed for elastic- and inelastic-storage values to be incorporated into a three-dimensional ground-water flow model (Trescott, 1975). After the development of the three-dimensional MODFLOW ground-water flow model (McDonald and Harbaugh, 1988), Leake and Prudic (1991) wrote a one-dimensional subsidence program for MODFLOW called the Interbed Storage Package (IBS1). This subsidence model is more versatile than the Meyer and Carr (1979) model and is used today as the standard for modeling subsidence in ground-water basins. Although this program does not contain the stress-dependent parameter capabilities of the earlier Helm model, it allows for continuous calculation of subsidence due to pumping in the areal extent of the model grid. Leake (1990) added other capabilities to the original code by allowing the evaluation of delayed drainage from interbeds within an aquifer system in an experimental version of the Interbed Storage Package (IBS2). Leake (1991) developed another Interbed Storage Package (IBS3) in which total load can be treated as a variable and storage parameters as stress dependent. These models can be used to evaluate vertical subsidence due to fluid withdrawal; however, they do not account for horizontal displacement resulting from changes in stress.

The surface effects of horizontal displacement have been evaluated by measuring radial strains (Wolff, 1970), by observance of failed surface structures (Poland and Davis, 1969) and through the presence of earth fissures (Holzer, 1984). Early explanations have associated the occurrence of horizontal movement with differential subsidence and compared the process to that of a bending beam failing at the point of greatest stress. That is, horizontal movement occurs primarily above the aquifer in the brittle unsaturated zone and is a direct consequence of vertical displacement. This theory does not apply to many fissures and structural failures that have been observed where minimal subsidence has been measured (Holzer, 1984; Anderson, 1989). In recent years, earth fissures have been shown to be directly related to horizontal aquifer movement due to pumping in unconsolidated aquifers (Helm, 1994a). In addition, many fissures are known to have migrated upwards from depth thus contradicting the earlier bending-beam theory of fissure development. Theoretical developments (Bear and Corapcioglu, 1981; Helm, 1994b) and field measurements of horizontal land-surface movement (Poland and Davis, 1969) indicate that

horizontal aquifer movement is significant and can be the same order of magnitude as vertical subsidence. Furthermore, Helm (1994b) indicates that horizontal movement due to pumping can occur beyond where measurable drawdown or subsidence occurs. Thus, the problems associated with land subsidence are three dimensional in scope. The calculation of both vertical and horizontal movement provides the necessary information water managers need to optimize pumping and reduce the potential for earth-fissure development. Earth fissures have resulted in many litigation cases because of structural damage caused to buildings, foundations, fences, railroads, roads, sidewalks, pipelines, and well casings. The next step in advancing the state of subsidence modeling is to include the mathematics needed to produce a model capable of simulating both horizontal and vertical aquifer-system deformation.

Development of a tractable field-based three-dimensional displacement model to simulate aquifer-system response to changes in applied stress is the next goal. Earlier subsidence models cannot provide the foundation for a three-dimensional displacement model because three-dimensional poroelastic theory is different from the theory used in one-dimensional subsidence models that are based solely on stress changes due to water-level declines. In Biot's (1941, 1955) development of three-dimensional consolidation (poroelastic) theory, the directional components of displacement and pressure or hydraulic head are dependent variables. This development incorporates the principle of effective stress and inherently assumes stress equilibrium and an elastic stress-strain constitutive relation. The resulting governing equation can be expressed as

$$(\lambda + G)\nabla(\nabla \bullet \boldsymbol{u}_s) + G\nabla^2 \boldsymbol{u}_s = \rho_w g \nabla h \ , \qquad (3)$$

where ρ_w is the density of water, g is the gravitational constant, h is hydraulic head, $\boldsymbol{u}_s$ is the displacement field of solids, G is the shear modulus (and one of Lamé's constants), and λ is the other Lamé constant. Lamé's constant λ is defined in terms of the shear modulus G and Poisson's ratio ν as

$$\lambda = \frac{2G\nu}{1-2\nu}, \qquad (4)$$

Equation (1) represents a system of three equations with four unknowns. Another equation is needed that relates hydraulic head to the displacement field of solids. The fourth equation is obtained by first writing Darcy's Law in terms of the velocity of solids,

$$n(\upsilon_w - \upsilon_s) = -\kappa \nabla h \ , \qquad (5)$$

where υ_w is the velocity of water, υ_s is the velocity of solids, κ is hydraulic conductivity, and n is porosity. Assuming constant water and solid-grain density, applying the principle of conservation of fluid and solid mass, taking the divergence of all the terms of equation (3), and relating volume strain to displacement yields the fourth equation,

$$\frac{\partial}{\partial t}(\nabla \bullet \boldsymbol{u}_s) = \kappa \nabla^2 h \ . \qquad (6)$$

Equations (1) and (4) are Biot's fundamental expressions of consolidation and have been used by P.A. Hsieh (see paper entitled "Poroelasticity Simulation of Ground-Water Flow and Subsurface Deformation, p. 5, this report) for developing a two-dimensional axisymmetric finite-element displacement model (referred to in this report as HDM).

Capabilities for simulating three-dimensional poroelasticity combined with the power and flexibility of MODFLOW would result in a valuable tool for analysis of aquifer deformation. Equation (4), however, is not compatible with MODFLOW, which uses specific storage instead of displacement or strain. Rice and Cleary (1976) use an alternative formulation of poroelastic theory. Their governing equation can be expressed as

$$\frac{\partial h}{\partial t} - \kappa\left(\frac{3\lambda + 2G}{3\rho_w g}\right)\nabla^2 h = \frac{1}{\rho_w g}\ \frac{\partial(\delta\sigma_m)}{\partial t} \ , \qquad (7)$$

where $\rho\sigma_m$ is the incremental change in mean total stress. Skeletal specific storage (S_s) for three-dimensional problems is defined as

$$S_s = \frac{3\rho_w g}{3\lambda + 2G} \ . \qquad (8)$$

Where and when the change in mean total stress appropriately is assumed to be negligible within a ground-water basin, equation (5) becomes identical to the traditional ground-water flow equation used in MODFLOW and other ground-water flow models. Assuming the change in mean total stress is negligible may eliminate the ability to simulate reversals of direction of change in water levels (Noordbergum effect) frequently observed during early times of pumping. None- theless, using this traditional expression with equation (1) results in a powerful coupling of equations to simulate three-dimensional consoli- dation (referred to here as the granular displace- ment model, or GDM) and three-dimensional ground-water flow within MODFLOW. Because basin-wide subsidence studies generally involve long time periods (simulation time of decades with individual time steps of a month or more), the change in mean total stress and the occurrence of reversals of direction of change in water levels probably are less significant. Neglecting the change in mean total stress, therefore, may not significantly affect results for long-term basin-wide simulations.

To evaluate the legitimacy of this approach, the HDM and GDM models are compared for three periods assuming an isotropic, confined-aquifer system with zero-displacement boundaries along the bottom and sides and a zero-traction boundary (zero total load) at the aquifer top. The side or lateral boundaries are more than 10,000 m from the pumping well and do not affect simulation results. Aquifer properties and initial conditions used in the simulations are shown in table 1. The calculated vertical and horizontal displacements resulting from the two models are shown in figures 1 and 2. Results indicate that for modeling aquifer-system displacements due to fluid withdrawal, the change in mean total stress may not be large, even for short time steps. Results indicate that the small, simulated differences in horizontal displacement may be due to the different numerical schemes or coordinate systems used in the two models. The GDM is an improvement over other models because it offers the power and flexibility of MODFLOW with the ability to simulate aquifer-system deformation in three dimensions. This model will help provide a better understanding of location and severity of potentially damaging fissures.

REFERENCES CITED

Anderson, S.R., 1989, Potential for aquifer compaction, land subsidence, and earth fissures in Avra Valley, Pima and Pinal Counties, Arizona: U.S. Geological Survey Hydrologic Investigations Atlas HA–718, 3 sheets, scale 1:250,000.

Bear, Jacob, and Corapcioglu, M.Y., 1981, Mathematical model for regional land subsidence due to pumping—2. Integrated aquifer subsidence equations for vertical and horizontal displacements: American Geophysical Union, Water Resources Research, v. 17, no. 4, p. 947–958.

Biot, M.A., 1941, General theory of three-dimensional consolidation: Journal of Applied Physics, v. 12, p. 155–164.

— 1955, Theory of elasticity and consolidation for a porous anisotropic solid: Journal of Applied Physics, v. 26, p. 182–185.

Gambolati, Giuseppe, Gatto, Paolo, and Freeze, R.A., 1974, Mathematical simulation of the subsidence of Venice—2. Results: American Geophysical Union, Water Resources Research, v. 10, no. 3, p. 563–577.

Helm, D.C., 1975, One-dimensional simulation of aquifer system compaction near Pixley,

Table 1. Aquifer properties and initial conditions used in the simulations to produce the results shown in figures 1 and 2

Property or condition	Value
Pumping rate, *Q*, in cubic meters per second	6.3×10^{-3}
Hydraulic conductivity, κ, in meters per second	1×10^{-4}
Drained Poisson's ratio, ν, dimensionless	.25
Shear modulus, *G*, in Newton per square meter	6.533333×10^{6}
Specific weight of water, $\rho_w g$, in Newton per cubic meter	9.8×10^{3}
Lamé's constant, λ, in Newton per square meter	6.533333×10^{6}

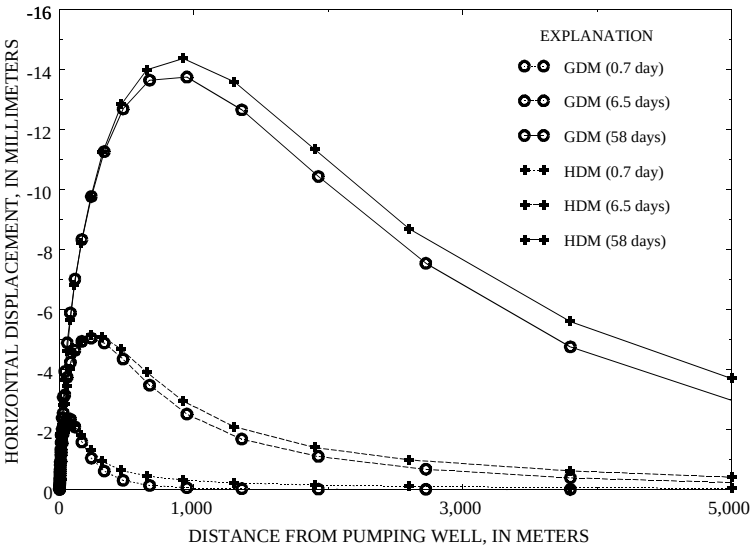

Figure 1. Simulated horizontal displacement for three time periods using the granular displacement model (GDM) and the Hsieh displacement model (HDM).

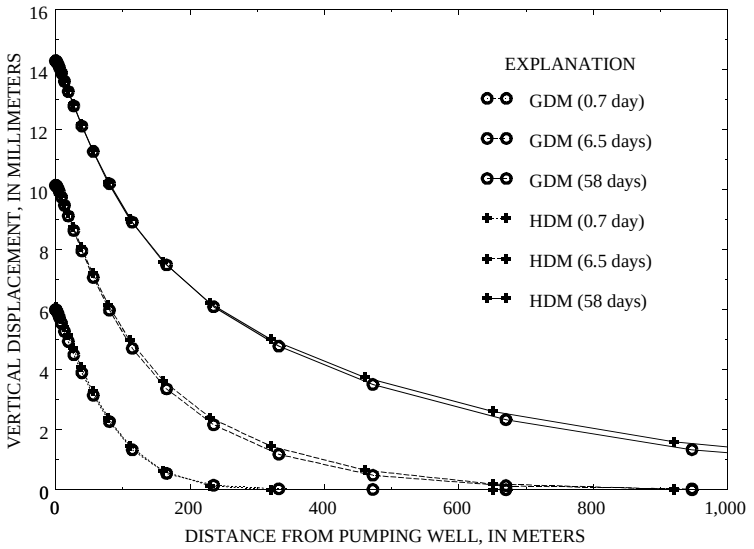

Figure 2. Simulated vertical displacement for three time periods using the granular displacement model (GDM) and the Hsieh displacement model (HDM).

California—1. Constant parameters: American Geophysical Union, Water Resources Research, v. 11, no. 3, p. 465–478.

___1976, One-dimensional simulation of aquifer system compaction near Pixley, California—2. Stress-dependent parameters: American Geophysical Union, Water Resources Research, v. 12, no. 3, p. 375–391.

___1994a, Hydraulic forces that play a role in generating fissures at depth: Bulletin of the Association of Engineering Geologists, v. 31, no. 3, p. 293–303.

___1994b, Horizontal aquifer movement in a Theis-Thiem confined system: American Geophysical Union, Water Resources Research, v. 30, no. 4, p. 953–964.

Holzer, T.L., 1984, Ground failure induced by ground-water withdrawal from unconsolidated sediment: Geological Society of America, Reviews in Engineering Geology, v. 6, p. 67–105.

Leake, S.A., 1990, Interbed storage changes and compaction in models of regional ground-water flow: American Geophysical Union, Water Resources Research, v. 26, no. 9, p. 1939–1950.

___1991, Simulation of vertical compaction in models of regional ground-water flow, *in* Johnson, I.A., ed., Land Subsidence: International Association of Hydrological Sciences Publication 200, Proceedings of the Fourth International Symposium on Land Subsidence, p. 565–574.

Leake, S.A., and Prudic, D.E., 1991, Documentation of a computer program to simulate aquifer-system compaction using the modular finite-difference ground-water flow model: U.S. Geological Survey Techniques of Water-Resources Investigations, book 6, chap. A2, 68 p.

McDonald, M.G., and Harbaugh, A.W., 1988, A modular three-dimensional finite-difference ground-water flow model: U.S. Geological Survey Techniques of Water-Resources Investigations, book 6, chap. A1, 586 p.

Meyer, W.R., and Carr, J.E., 1979, A digital model for simulation of ground-water hydrology in the Houston area, Texas: Texas Department of Water Resources Report LP–103, 27 p.

Poland, J.F., and Davis, G.H., 1969, Land subsidence due to withdrawals of fluids, *in* Varnes, D.J., and Kiersch, George, eds., Reviews in Engineering Geology—Volume 2: Boulder, Colorado, Geological Society of America, p. 187–269.

Rice, J.R., and Cleary, M.P., 1976, Some basic stress diffusion solutions for fluid-saturated elastic porous media with compressible constituents: Review of Geophysics and Space Physics, v. 14, p. 227–241.

Trescott, P.C., 1975, Documentation of finite-difference model for simulation of three-dimensional ground-water flow: U.S. Geological Survey Open-File Report 75–438, 32 p.

Wolff, R.G., 1970, Relationship between horizontal strain near a well and reverse water-level fluctuation: American Geophysical Union, Water Resources Research, v. 6, no. 6, p. 1721–1728.

Deformation of a Sandbar in Response to Changes in Effective Stress Along the Colorado River in the Grand Canyon, Arizona

By M.C. Carpenter

Discharge from Glen Canyon Dam on the Colorado River can fluctuate from about 85 to 800 m^3/s on a daily basis. Corresponding river-stage fluctuations on downstream beaches can exceed 3.4 m. Rill erosion, slumping, and fissuring on seepage faces of many sandbars observed at low river stage are a response to ground-water flow caused by residual hydraulic-head gradients in the sandbars, which is the result of river-stage fluctuation.

From April 1991 to March 1993, a sandbar was instrumented with sensors for continual monitoring of river stage, pore pressure, temperature, and biaxial tilt to determine relations among ground-water flow, changes in effective stress, seepage stresses, and sandbar deformation. Five clusters of deep, intermediate, and shallow pairs of pore-pressure and temperature sensors were installed in a vertical plane orthogonal to the river's edge. The clusters were spaced a few meters apart in the sandbar face above, within, and below the zone of fluctuating river stage to determine the vertical component of ground-water flow in the deforming sandbar face. The clusters were spaced more than 10 m apart in the middle and back of the sandbar. Seven tilt sensors were installed parallel with and orthogonal to the river's edge in the deforming sandbar face.

The sandbar consisted of homogeneous fine to medium sand overlying medium sand at a depth of 6 m. The back boundary was talus with a narrow, deep, return channel underlain by a thin clayey silty sand. The zone of fluctuating river stage was a steeply sloping face that exhibited rill erosion, slumping, and fissuring.

A sequence of tilts occurred from July 7, 1991, through July 17, 1991. The tilts were at least five times greater orthogonal to the river than parallel to the river. The sign convention for tilts ortho- gonal to the river is positive for tilts upward toward the river and negative for tilts downward toward the river. On July 7, a tilt of 5.5∞° occurred orthogonal to the river. On July 12, a tilt of -0.5°∞ occurred; and on July 17, an additional tilt of -3.3°∞ occurred. These major occurrences were followed by continued negative tilt orthogonal to the river from July 18 to July 26, punctuated with daily spikes of about -0.4°π. All sudden tilts occurred on downward limbs of the daily hydrographs when the effective stress (intergranular stress) in the sandbar face was increasing. The hypothesis sug- gested is a slump-creep sequence: (1) outward- flowing ground water caused oversteepening of the lower part of the slope in the zone of fluctuating river stage by rilling; (2) slumping (rotational failure) of the metastable slope was triggered by increased effective stress; and (3) leveling of the slightly uplifted mound on the toe slope of the slump block occurred by downslope creep.

Piezometric-Extensometric Estimations of Specific Storage in the Albuquerque Basin, New Mexico

By Charles E. Heywood

Appropriate values of skeletal specific storage (S_{sk}) and hydraulic conductivity are required for numerical simulations to achieve useful predictions of ground-water level responses to future pumping. These parameters often are estimated from the measured hydraulic response to short-duration pumping tests, which may effectively stress only the more permeable parts of the aquifer system within a previously stressed magnitude range. Because the magnitude of S_{sk} may depend on the time period of the applied hydraulic stress as well as the stress history of the aquifer system (Helm, 1976; Galloway, 1995), estimates of S_{sk} from such tests often are applied inappropriately in ground-water flow simulations for systems with significant low-permeability lithologies or a component of inelastic compressibility.

Early in a test close to the pumped well, horizontal strain of the aquifer matrix may induce appreciable pore-pressure changes before the hydraulic propagation of drawdown. Such effects were observed in the test described in this paper. Analytical solutions of radial ground-water flow problems are most sensitive to the storage coefficient (S) during early time and typically are based on models that neglect horizontal strain. If piezometric data close to the pumped well are analyzed with such a model, erroneous parameter estimates may result. For these reasons, direct in-situ measurement of vertical aquifer-system matrix compressibility is preferable for estimating aquifer-system specific storage.

In the Albuquerque Basin of New Mexico, ground-water withdrawals result in depletion of aquifer-system storage and of surface-water flow in the Rio Grande. Because the economics and administration of these water sources differ, an improved understanding of ground-water and surface-water interaction near the Rio Grande was desired, and an aquifer test was carried out during the winter of 1995. A 3-month recovery period preceded 54 days of pumping at about 147 L/s, which was followed by a 1-month recovery period. The production well was screened from 71 to 244 m; however, post-test televiewing and flow-metering revealed that the screen was encrusted and did not produce significant water below 195 m (Condé Thorn, hydrologist, U.S. Geological Survey, oral commun., 1995).

Before the test in the fall of 1994, a 315-meter borehole extensometer was installed 378 m from the test well as part of an effort to monitor aquifer-system compaction that would result in land subsidence. This counter-weighted borehole-pipe extensometer design followed guidelines described by Riley (1984) to achieve high-strain sensitivity. A precision transducer measures vertical displacements with a resolution of several microns corresponding to a vertical-strain sensitivity of 10^{-8}. A nest of four piezometers was installed 5 m from the extensometer and equipped with transducers capable of detecting 2 mm of water-level change. During the aquifer test, water levels also were recorded in three shallower piezometers approximately 80 m from the extensometer and in 12 other observation wells at various distances farther from the pumped well. The electrical-resistivity borehole-geophysical log illustrates the depth and thickness of sand and clay interbeds of the aquifer-system interval penetrated by the extensometer (fig. 1). Clay and silt layers correlate with lower resistivity. Piezometer screens were placed in high-resistivity intervals that were assumed to be sands of high permeability.

The relation between aquifer pore-pressure decrease and vertical strain for the period of drawdown and subsequent recovery is shown in figure 2. Pore pressure was measured 6 m from the

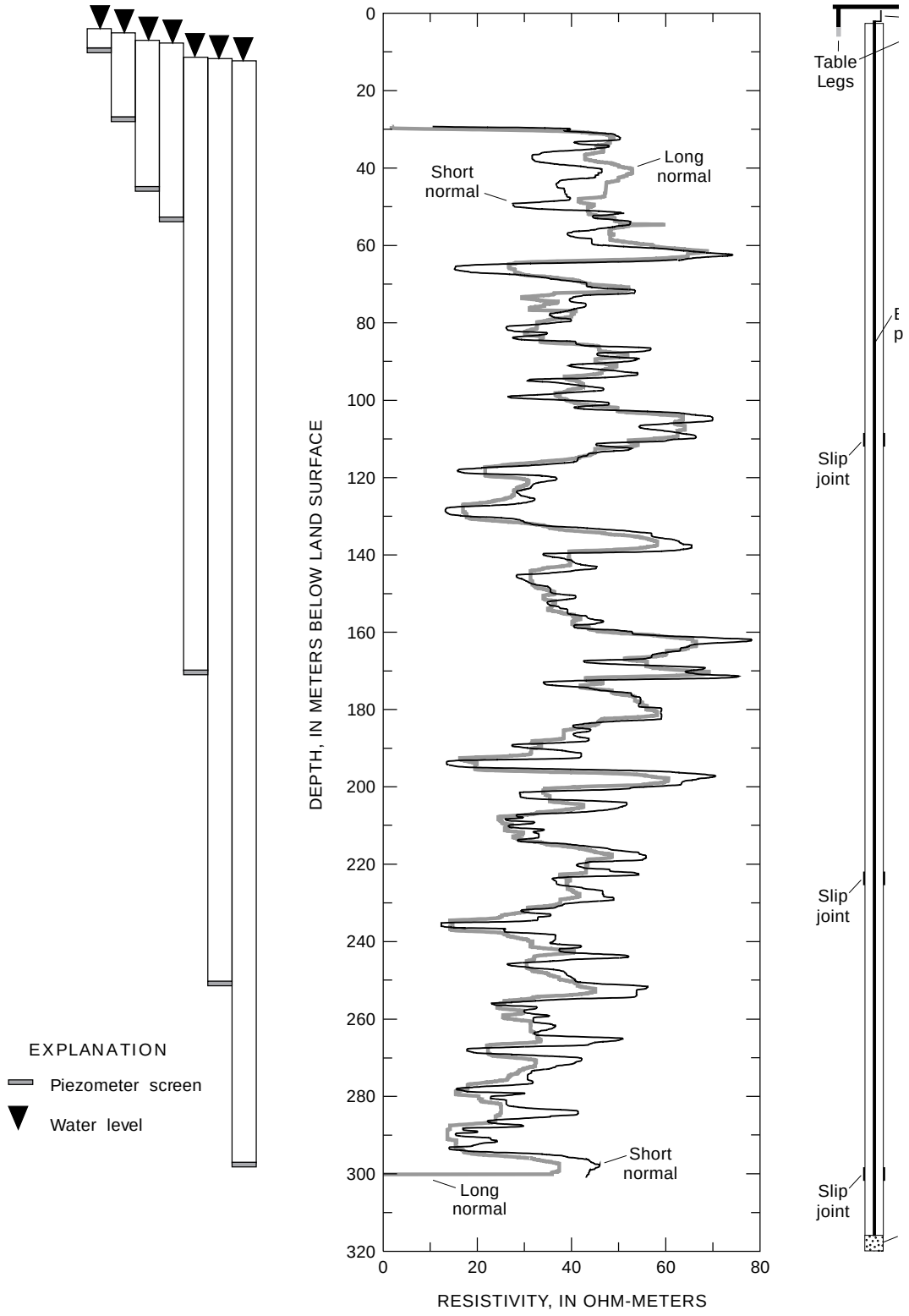

Figure 1. Summary of Montaño extensometer-piezometer installation.

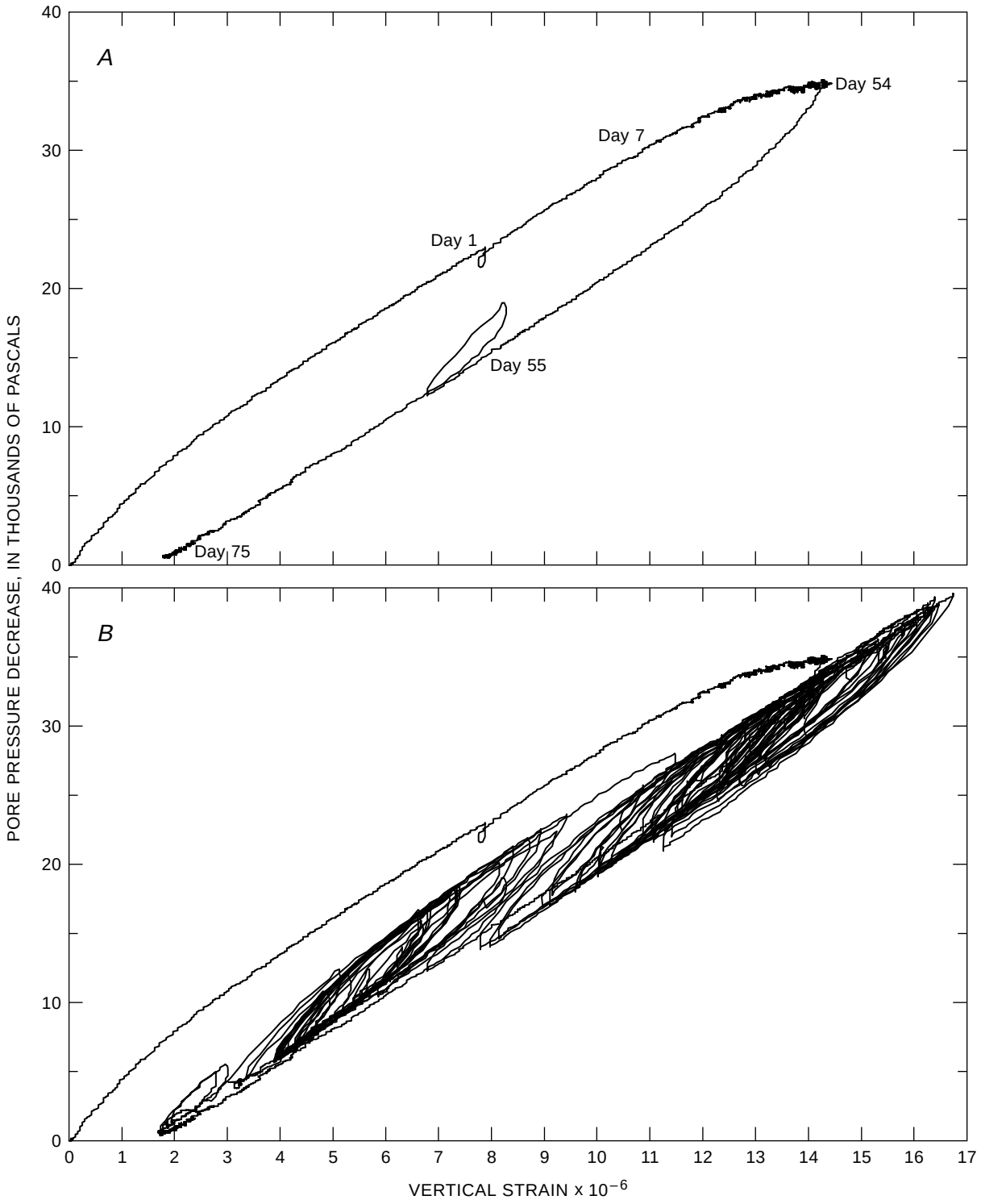

Figure 2. Pore-pressure change at a depth of 171 meters compared to aquifer-system strain. *A*, Test-pumping and recovery period. *B*, Test-pumping and recovery period and subsequent period of uncontrolled pumping at multiple wells.

extensometer at a depth of 171 m, and vertical strain was measured over the interval of the extensometer (fig. 1). A 27-minute pump failure that occurred 1 day into the aquifer test caused measurable elastic recovery at the extensometer and resulted in a small loop in the plot. An analogous effect was observed on day 55 when the pumped well was inadvertently turned back on for about 2 hours. Piezometer hydrographs flattened approximately 1 week into the drawdown and recovery periods of the test and indicate that drawdown approached steady state in permeable parts of the aquifer system where piezometers were screened. As shown in figure 2*A*, the flatter slope from day 7 to day 54 probably reflects compaction of interbedded sediments of low permeability as they slowly drained excess pore pressure to the surrounding aquifer. This decrease in slope also may be due to apparent strain attributable to uncompensated long-period temperature effects in the extensometer apparatus. The controlled-test data from figure 2*A* and an additional 60 days of superimposed post-test data are shown in figure 2*B*. During the latter 60 days, normal "uncontrolled" pumping from multiple wells near the extensometer resulted in many drawdowns of various magnitudes on a daily basis. The stress-strain plot during this period is shifted to the right of the plot for the controlled test suggesting that (1) some inelastic compaction resulted from the test, (2) an uncompensated temperature effect on the extensometer has resulted in apparent strain, or (3) the recovery period was 39 percent of the drawdown period, which was insufficient for the pore pressure in less permeable parts of the aquifer system (above or below the piezometer screened at 171 m) to return to prepumping levels. Since the late 1950's, production wells near the extensometer generated approximately diurnal drawdowns of a similar magnitude to drawdowns generated in the aquifer test; however, it is possible that the aquifer system has not experienced that magnitude of constant drawdown for a period as long as the aquifer test (54 days). During the aquifer test, the middle of the thick interbeds of low permeability may have had more time to drain excess pore pressure than at any previous time resulting in effective stress magnitudes above a precon- solidation level in the middle of the interbeds. Resulting inelastic compaction totaling 0.45 mm would generate the apparent inelastic strain shown in figure 2*B*. Additional seasonal stress-strain and temperature data will enable discrimination of these three possibilities for the right shift of the stress-strain plot.

Riley (1969) demonstrated the utility of similar stress-strain plots for determining elastic- and inelastic-storage coefficients. The magnitude of the inverse slope of this stress-strain plot would be a measure of the compressibility of the average aquifer matrix over the interval spanned by the extensometer if the change in pore pressure were uniform in that interval. The distribution of aquifer-system pore-pressure change was sampled with piezometers over seven depth intervals. Sample hydrographs, in conjunction with the vertical-permeability distribution inferred from the borehole-resistivity log, were used to estimate the change in vertical pore-pressure distribution during the aquifer test. The average pore-pressure change over the sampled aquifer-system interval was approximated by the average drawdown recorded in the four deepest piezometers. For the aquifer-system interval spanned by the extensometer, the resulting estimated matrix compressibility, α, is 5×10^{-10} Pa^{-1}. For an average matrix porosity, n, of 0.3 and water compressibility, β, of 4.4×10^{-10} Pa^{-1}, the corresponding specific storage, S_s, $[\rho g(\alpha+n\beta)]$ is 7×10^{-6} m^{-1}, where the weight density of water, ρg, is 9,800 kg m^{-2} s^{-2}.

The shallowest piezometer near the extensometer was screened across the water table. During the pumping period of the test, the water-table elevation recorded in this well declined less than 0.3 m. Assuming a specific yield of 0.2, the resulting decrease in geostatic stress on underlying sediments was less than 6×10^{2} Pa. Measured pore pressure decreased by 3.6×10^{4} Pa in the piezometer at a depth of 171 m and by somewhat less in the piezometers screened at other depths. For sediments in the producing aquifer interval (from a depth of approximately 60 to 200 m), the magnitude of decreased effective stress resulting from water-table lowering, therefore, was on the order of 2 percent of the increased effective stress due to decreased pore pressure. Because the effect of water-table lowering on effective stress at depth generally was minor during the aquifer test, the water table was assumed to be static. A unit

decrease in measured pore pressure, therefore, corresponded to a unit increase in effective stress.

Piezometric responses to earth tides enabled an independent estimation of specific storages of the aquifer sands surrounding each piezometer screen. Three 3-week series of hourly pressure data were filtered to pass frequencies between 0.8 and 3.0 cycles/d by a digital 9th order elliptic filter with 0.01 decibels of ripple in the passband and a stop band that was 100 decibels lower than the peak value in the passband. The theoretical magnitude of volumetric strain due to earth tides was calculated from tidal theory (Harrison, 1971) assuming a Poisson ratio of 0.25. The magnitudes of aquifer volumetric strain and resulting piezometric responses at six principal tidal frequencies were determined by Fourier regression from which values of S_s were calculated for the M2 and O1 frequencies by assuming grain incompressibility (Bredehoeft, 1967). Figure 3 shows the mean S_s calculated from the M2 tidal response compared to screen depth for the four deepest piezometers adjacent to the extensometer (darker circles and lines). Error-bar widths are 2 standard deviations. These values of S_s are smaller than that of the aggregate aquifer system and suggest that aquifer sands are stiffer than the aquifer system, which includes interbedded clay aquitards. The data suggest that sand-matrix compressibility decreases approximately linearly with increasing overburden stress. Open circles representing a similar analysis (Heywood, 1995) of two piezometers in a similar setting in El Paso, Texas, follow a similar trend. Barometric efficiency (BE) was estimated as a function of frequency (Rojstaczer, 1988) for the Albuquerque piezometers and was found to be about 0.2 in the tidal-frequency range. This magnitude of BE and estimated S_s suggests sand-matrix porosities of about 0.3. The flat frequency response in the tidal spectrum suggests that piezometric earth-tide responses probably are not significantly attenuated by pressure diffusion.

REFERENCES CITED

Bredehoeft, J.D., 1967, Response of well-aquifer systems to earth tides: American Geophysical Union, Journal of Geophysical Research, v. 72, no. 12, p. 3075–3087.

Galloway, D.L., 1995, The frequency dependence of aquifer-system elastic storage coefficients—Implications for estimates of aquifer hydraulic

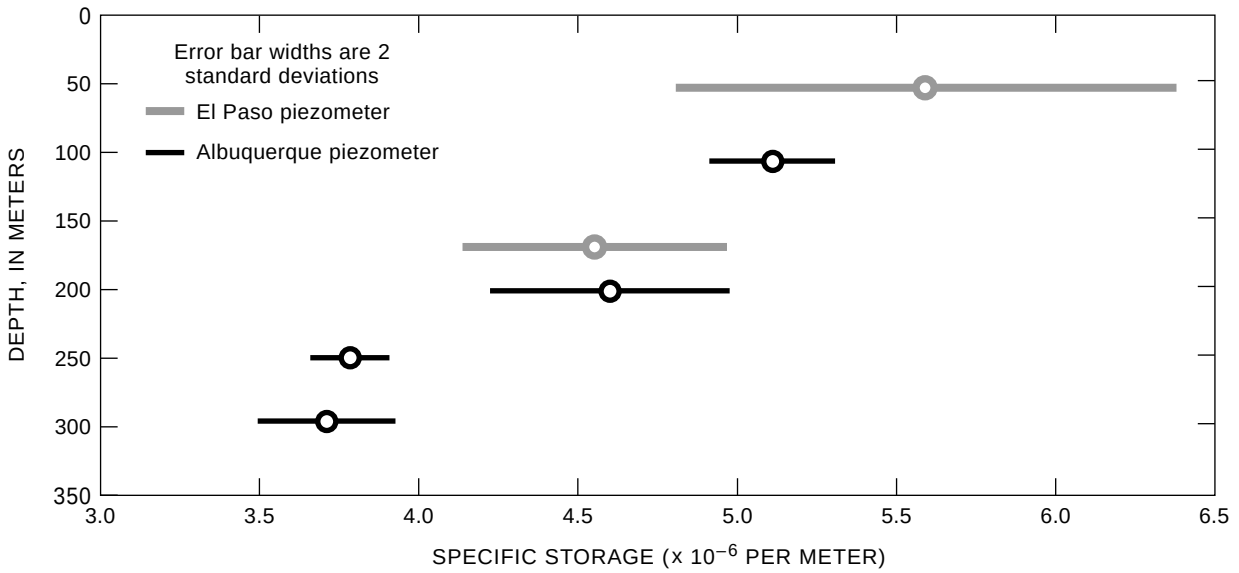

Figure 3. Specific storage for aquifer sands in Rio Grande alluvium from M2 tidal response.

properties and aquifer-system compaction, *in* Prince, K.R., Galloway, D.L., and Leake, S.A., eds., U.S. Geological Survey Subsidence Interest Group Conference, Edwards Air Force Base, Antelope Valley, California, November 18–19, 1992—Abstracts and Summary: U.S. Geological Survey Open-File Report 94–532, 84 p.

Harrison, D.H., 1971, New computer programs for the calculation of earth tides: Boulder, University of Colorado, Cooperative Institute for Research in Environmental Sciences.

Helm, D.C., 1976, One-dimensional simulation of aquifer system compaction near Pixley, California 2.—Stress dependent parameters: American Geophysical Union, Water Resources Research, v. 12, no. 3, p. 375–391.

Heywood, C.E., 1995, Investigation of aquifer-system compaction in the Hueco basin, El Paso, Texas, USA, *in* Proceedings of the Fifth International Symposium on Land Subsidence: International Association of Hydrological Sciences Publication 234, p. 35–45.

Riley, F.S., 1969, Analysis of borehole extensometer data from central California, *in* Tison, L.J., Land Subsidence: International Association of Hydrological Sciences Publication 89, v. 2, p. 423–431.

__ 1984, Developments in borehole extensometry, *in* Johnson, A.I., Carbognin, L., and Ubertini, L., eds, Land Subsidence: International Association of Hydrological Sciences Publication 151, p. 169–186.

Rojstaczer, S.A., 1988, Determination of fluid flow properties from the response of water wells to atmospheric loading: American Geophysical Union, Water Resources Research, v. 24, no. 11, p. 1927–1938.

Results of Global Positioning System Surveys in Antelope Valley, California

By Marti E. Ikehara

Land subsidence has been occurring in Antelope Valley, California, because of a long history of ground-water pumping that has exceeded natural recharge. Water demand is expected to increase rapidly with the projected increase in population from about 320,000 in 1994 to about 600,000 by the year 2010 (Templin and others, 1995). Much of this demand probably will be met through increased ground-water with- drawal. The flexibility of accurately measuring land-surface elevations of bench marks distributed at both regional and local-scale spacing can be achieved by Global Positioning System (GPS) surveying. A static survey of 85 geodetic stations throughout Antelope Valley and a kinematic survey of 85 stations concentrated along a 4-mile-long (6.4-kilometer) rocket-testing track at Edwards Air Force Base were done using GPS surveying. The objectives of the first survey were to measure current land-surface elevations for calculations of historical land subsidence and to establish ellipsoidal heights for future subsidence monitoring using repeated GPS measurements. The objective of the second survey was to establish horizontal and vertical positions for crustal-motion monitoring before the onset of pumping at new ground-water wells along the track.

Antelope Valley is in the western part of the arid Mojave Desert in southern California and is about 50 mi (80 km) northeast of Los Angeles. The triangular-shaped valley is bounded on the south by the southeastward-trending San Gabriel Mountains, on the northwest by the northeastward-trending Tehachapi Mountains, and by smaller ridges and buttes to the north and east. Antelope Valley is considered high desert, and elevations of the valley floor range from about 2,260 to 2,950 ft (690 to 900 m) above sea level. The valley is a topographically closed basin, and surface-water drainage terminates in several playas—the most notable of which are Rogers and Rosamond Lakes. Fine-grained sedimentary deposits predominate in the center of the basin and within the Lancaster ground-water subbasin, which is the source of much of the valley's water.

In the spring of 1992, the regional-scale GPS survey of 85 stations in Antelope Valley was carried out using from four to seven receivers simultaneously (Ikehara and Phillips, 1994). Dual-frequency signals were recorded at 15-second intervals for 5- to 7-hour durations at each station. The network included 7 horizontal-control stations and 10 stable vertical-control stations and resulted in 332 vectors, or relative-position coordinates, between two simultaneously observed bench marks. The least-squares adjustment in which coordinates for all control stations were held fixed produced a vertical-standard error (2σ) that ranged between 0.03 and 0.081 ft (0.9 and 2.4 cm) and averaged 0.05 ft (1.5 cm). The maximum error associated with the geoid model (GEOID90) used to compute orthometric heights (elevations) in this survey was about 0.2 ft (6 cm), as determined by a comparison with recent leveling for a 20.3-mile (32.7-kilometer) line along Sierra Highway between gravity and topographic highs and lows in the valley (fig. 1).

Between about 1930 and 1992, the maximum calculated magnitude of subsidence was more than 6.0 ft (1.83 m) in Lancaster, the largest city in Antelope Valley (fig. 2). Estimates of subsidence at other nearby bench marks, partially based on estimated values for the period before 1960, are as high as 6.6 ft (2.01 m). Between Lancaster and Redman, which is a predominantly agricultural area 12.5 mi (20 km) to the northeast, 4 ft (1.22 m) or more of subsidence has been measured at bench marks (fig. 2).

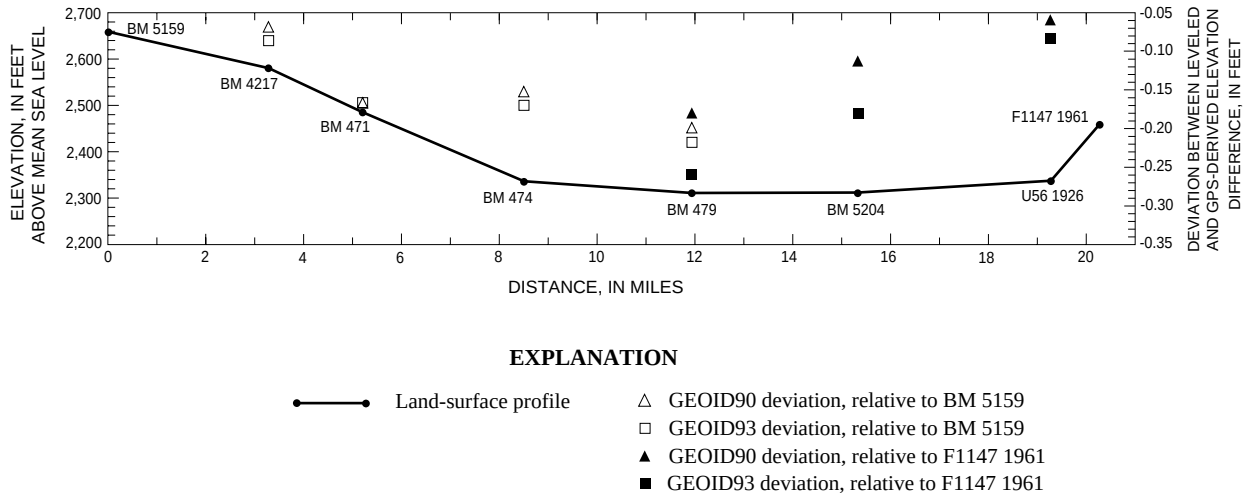

Figure 1. Land-surface profile on Sierra Highway between Palmdale and Rosamond and error for Global Positioning System-derived elevation differences relative to leveled differences of bench-mark pairs (modified from Ikehara and Phillips, 1994, fig. 1).

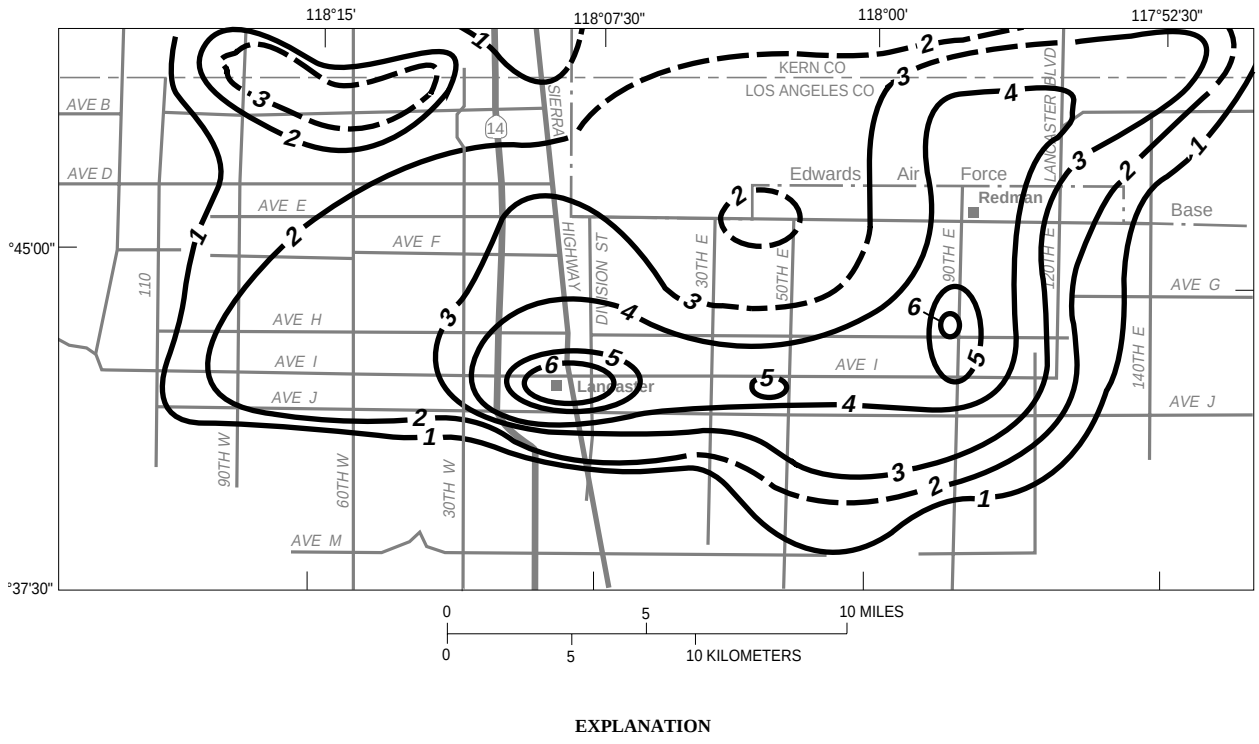

Figure 2. Magnitude of calculated or estimated subsidence in central Antelope Valley, 1930 to 1992 (modified from Ikehara and Phillips, 1994, fig. 8).

Land subsidence in Antelope Valley is caused by aquifer-system compaction that is related to water-level declines and the presence of fine-grained compressible sediments. The potentiometric surface and water-level declines of the Lancaster ground-water subbasin were mapped for several periods since the 1950's and compared to subsidence-rate maps. As expected, the correlation between water-level declines and the distribution and rates of subsidence were highest where compressible sediments were present generally toward the lowest parts of Antelope Valley. In contrast, areas, such as Palmdale, that are closer to the mountains and underlain by coarser sedimentary material showed little or no land subsidence even when water levels had declined tens of meters over decades.

The mechanics of land subsidence might be better understood if horizontal and vertical geodetic measurements of the land surface were made before as well as after the onset of stresses imposed on the aquifer. The establishment of a horizontal and vertical base line was accomplished by a recent local-scale geodetic survey of densely-spaced reference marks that was done before production in two new nearby ground-water wells. A kinematic GPS survey of 82 reference stations was done in August 1994 at a straight, 4-mile-long (6-kilometer-long) abandoned track that was built for testing rocket sleds at Edwards Air Force Base in the northeastern part of Antelope Valley. For the first part of the survey, the two nearest stable vertical-control stations that are part of the regional-scale network established in 1992 were observed in static mode simultaneously with the

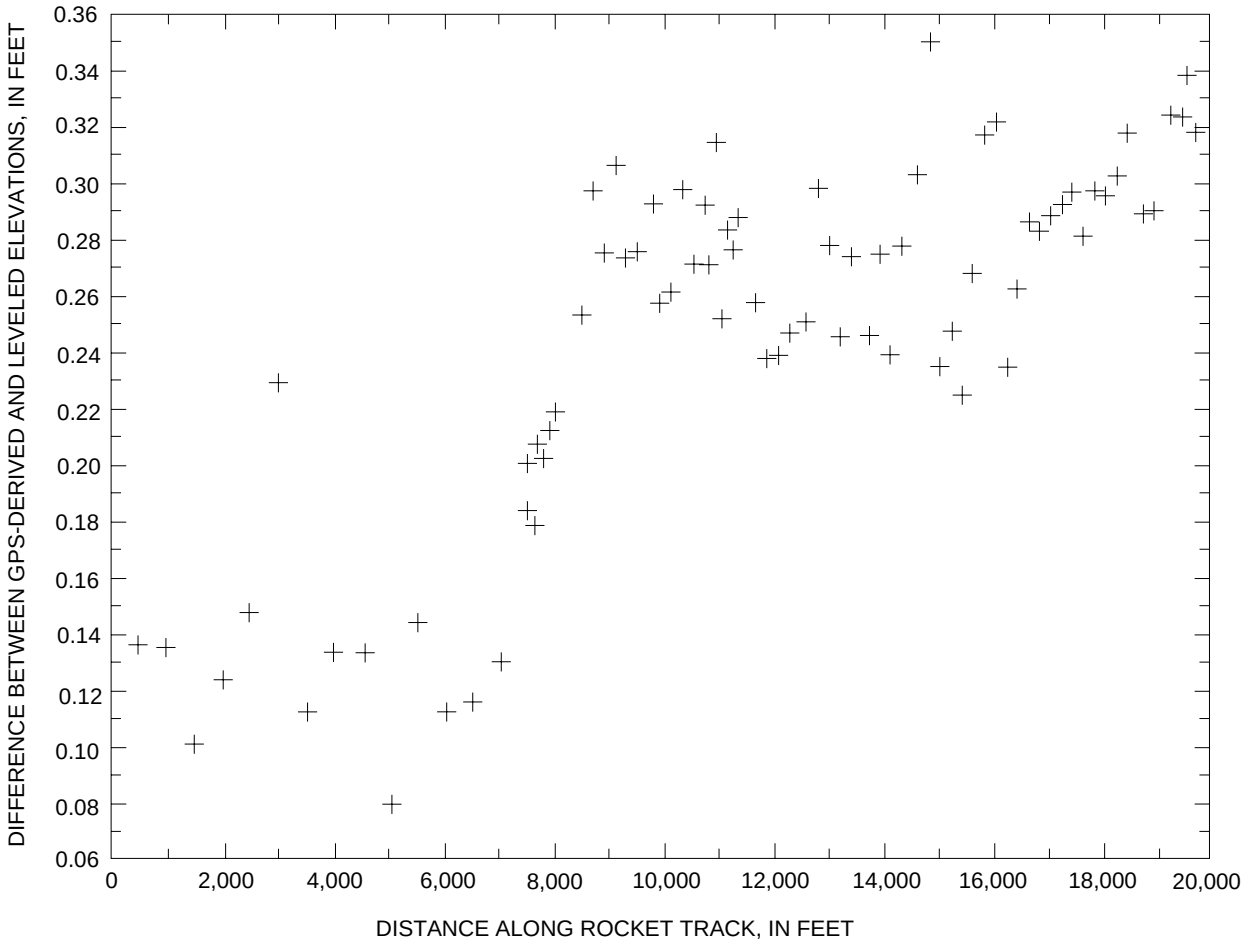

Figure 3. Comparison of Global Positioning System-derived elevations relative to leveled elevations of rocket-track stations measured at Edwards Air Force Base, Antelope Valley, August 1994.

two base stations established for the kinematic survey. The static observations were made at 15-second intervals for 2 hours at the track stations; the kinematic observations were made at 10-second intervals for 15 epochs (2.5 minutes). In kinematic surveys, an offset to the base station, called a swap station, is established for use by the rover, which is the antenna that visits all stations for which coordinates are to be determined. During postprocessing, horizontal and vertical coordinates were computed for 2 base stations, 1 swap station, and 80 track stations.

A leveling survey that included most of the 80 track stations was done during the same week. The survey was not double run because of time constraints; however, the data allowed a general comparison between elevations obtained by GPS and leveling methods (fig. 3). Relative to leveled elevations, GPS-derived values differed by 0.08 to 0.35 ft (2.4 to 10.7 cm). One possible explanation for the bimodal distribution of elevation differences is that the base station for the track stations between 8,000 and 20,000 ft (2,438 and 6,096 m) was not included in the leveling. Although the leveled elevations are considered known for this comparison, unadjusted leveling error at the breakpoint—the switch between base stations—may account for the abrupt change in the differences. The GPS-computed positions and ellipsoidal heights would be used as the base-line values with which future geodetic measurements of track stations could be compared.

REFERENCES CITED

Ikehara, M.E., and Phillips, S.P., 1994, Determination of land subsidence related to ground-water-level declines using global positioning system and leveling surveys in Antelope Valley, Los Angeles and Kern Counties, California, 1992: U.S. Geological Survey Water-Resources Investigations Report 94–4184, 101 p.

Templin, W.E., Phillips, S.P., Cherry, D.E., DeBortoli, M.L., and others, 1995, Land use and water use in the Antelope Valley, California: U.S. Geological Survey Water-Resources Investigations Report 94–4208, 97 p.

Deformation in the Casa Diablo Geothermal Well Field, Long Valley Caldera, Eastern California

By James F. Howle *and* Christopher D. Farrar

Long Valley Caldera in eastern California has been the site of seismic swarms and deformation in response to magmatic intrusions since 1980 (Hill and others, 1985; Langbein, 1989; Langbein and others, 1993). Magmatic intrusions are causing regional uplift of the land surface across the resurgent dome and the Casa Diablo geothermal well field (figs. 1 and 2). Superimposed on the regional uplift is local subsidence in and around the well field caused by pumping of geothermal fluid. This paper presents a time-series overview of land-surface deformation in the well field and relates the deformation to the two principal sources of stress—magmatic inflation and pumping of geothermal fluid. Leveling data from three networks that overlap areally and temporally are presented beginning with the bench marks along Highway 395.

The Highway 395 long base-line network extends 65 km from Lee Vining to Tom's Place, California. Bench marks are spaced at intervals less than or equal to 1 km. Elevation changes for bench marks in the Highway 395 long base-line network for three periods between 1983 and 1992 are shown in figure 3. Elevation changes for 1983 to 1985 indicate uniform uplift across the well field that totals about 20 mm (Savage and others, 1987; Dan Dzurisin, geologist, U.S. Geological Survey, written commun., 1993). Elevation data for 1983 to 1985 provide a preproduction base line of the land surface and indicate that no significant subsidence occurred before geothermal fluid was pumped.

Electric-power generation using geothermal fluid in the Casa Diablo field began in 1985 with one powerplant (MP-1) that produced about 10 megawatt gross electric power (Mwe). All of the 0.8×10^6 kg/hr of fluid is pumped from wells and circulated through the MP-1 powerplant and

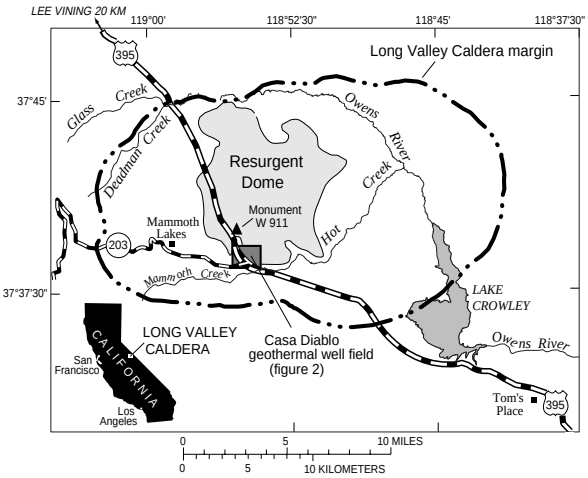

Figure 1. Location of Long Valley Caldera, California.

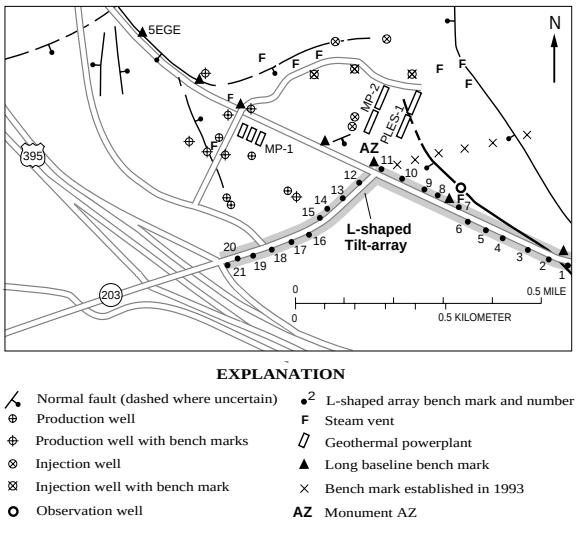

Figure 2. Casa Diablo geothermal well field, monument networks, and bounding normal faults.

returned to the subsurface through injection wells. Fluid with a temperature of about 170°C is pumped from a 150- to 200-meter-deep production zone and loses about 70°C in the heat-exchange process before it is injected into a zone 600 to 700 m deep.

Between 1985 and 1988, bench-mark elevation changes indicate that monument W911, 2 km north of the well field, moved up about 80 mm in response to regional inflation caused by magmatic intrusions (fig. 3). Monument AZ moved up only about 30 mm, which is equivalent to about 50 mm of local subsidence for that period. In figure 3, elevation change is for a particular period and is not cumulative from 1983. From 1983 to 1992, the cumulative elevation change for monument W911 is about 200 mm. All monuments within about 1 km of monument AZ subsided relative to the regional uplift and clearly define the extent of the localized subsidence caused by pumping of geothermal fluid along the Highway 395 long base line. For 1985 to 1988, subsidence related to geothermal pumping counters but does not entirely mask the regional uplift from magmatic intrusions.

In December 1990, two additional powerplants (MP-2 and PLES-1) became operational. About four times as much geothermal fluid is required to operate all three powerplants as was needed for MP-1 alone. Bench-mark elevation changes on the Highway 395 long base line between 1988 and 1992 (fig. 3) show that W911 was uplifted about 100 mm; however, monument AZ subsided about 20 mm. The increase in pumping from 0.8×10^6 kg/hr to 3.0×10^6 kg/hr caused the local area of subsidence to expand almost 2 km on either side of monument AZ (fig. 3) and completely masked regional uplift of monument AZ and nearby monuments.

The second leveling network is the L-shaped tilt array, a network of closely spaced monuments along two nearly perpendicular lines (fig. 2). Data from this network also show subsidence caused by pumping of geothermal fluids. Differences in monument elevations between consecutive surveys are resolved into north and east components of ground tilt. Data for the north component of tilt for 1984 to 1994 are shown in figure 4. Through 1984, the data show a tilt to the south of 5 μrad/yr in response to magmatic inflation north of the well field. The next leveling of the tilt array in 1985 revealed a reversal in the tilt direction as a result of the onset of geothermal production. Subsequent surveys through 1989 reveal a linear tilt rate of 38±2 μrad/yr to the north toward the well field.

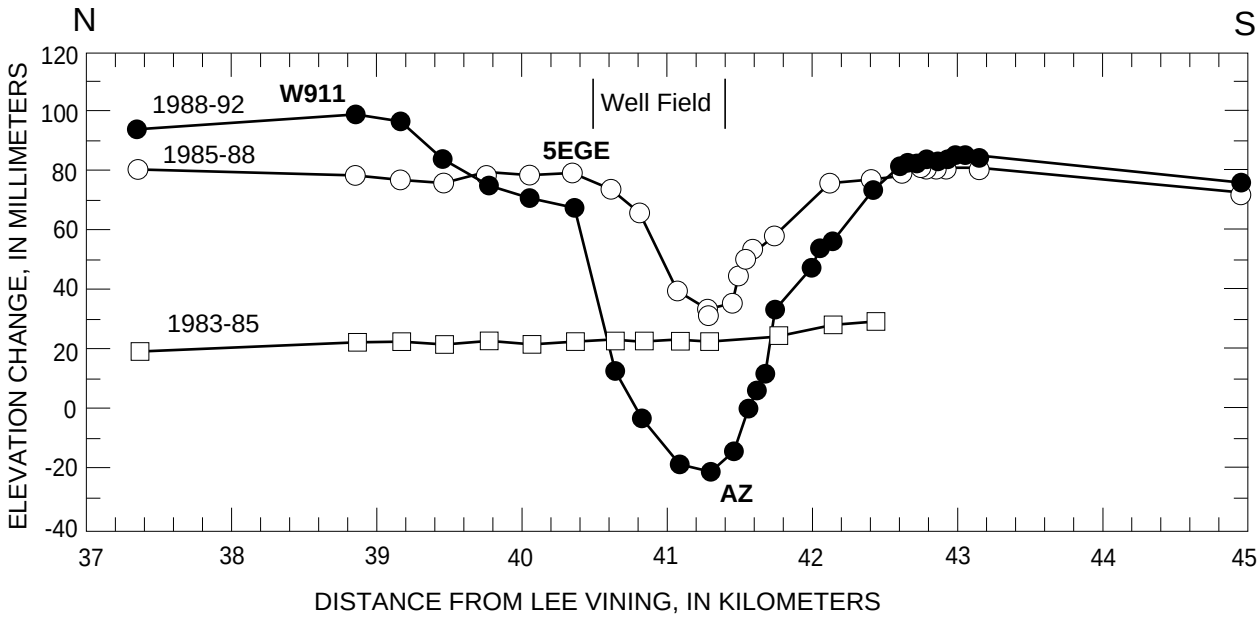

Figure 3. Elevation changes in the Highway 395 long base line for three periods between 1983 and 1992. Elevation change is for an individual period and is not cumulative from 1983 (modified from Sorey and others, 1995).

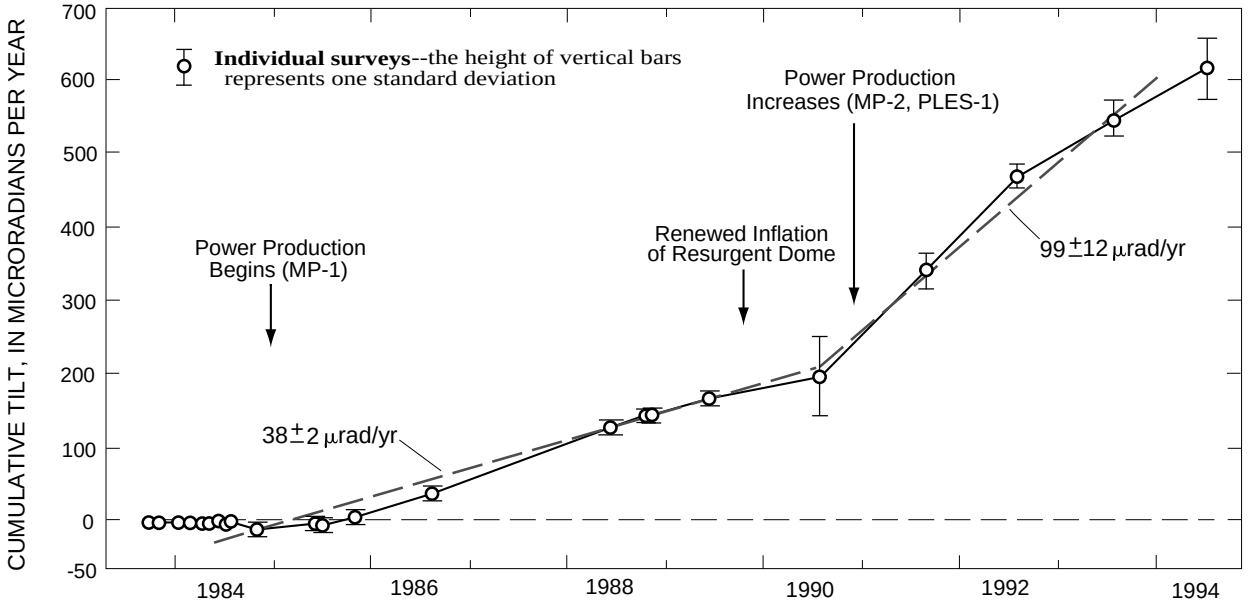

Figure 4. Cumulative land-surface tilt (modified from Sorey and others, 1995).

Renewed inflation of the resurgent dome in late 1989 (Langbein and others, 1993) could be the cause of the slight decrease in tilt observed between the 1989 and 1990 surveys. In December 1990, pumping was increased by 2.2×10^6 kg/hr to supply two additional powerplants (MP-2 and PLES-1). This increase in pumping nearly tripled the tilt rate into the well field. From 1990 to 1994, the north component is fit reasonably well by a linear rate of 99±12 μrad/yr.

In June 1988, the third leveling network was established to provide a more detailed picture of the deformation and consists of 45 monuments within the well-field graben and across the bounding faults. Data from this leveling network show significant changes in the location and magnitude of maximum subsidence in the well field between 1988 and 1994 (figs. 5*A*–*C*). The observed changes probably were caused by a combination of factors and processes including changes in pressure and temperature, infiltration of cold shallow ground water, venting of steam from the reservoir, variations in rock compressibilities, and changes in well locations and injection depths (Sorey and others, 1995). Prior to 1992, the area of maximum subsidence was 500 m east of the production wells that are centered around monument AZ (fig. 5*A*). The offset between the area of maximum reservoir pressure drop at the production wells and the area of maximum subsidence at monument AZ could have been caused by lateral differences in lithology. The production wells are completed in silicified rhyolite of low compressibility. The area around monument AZ, where subsidence is greatest, could be underlain by hydrothermally altered rhyolite, which is highly compressible.

Data collected in 1993 show that the area of maximum subsidence had shifted 500 m west of monument AZ and was centered around the production wells (fig. 5*B*). The change in location and magnitude of maximum subsidence resulted partly from pressure decreases in the production reservoir. A 10-meter decrease in head was caused by a pumping-rate increase to supply the two new powerplants in December 1990. In mid-1991, shallow perforated zones in the injection wells were sealed to prevent thermal breakthrough of the cooled injectate to the production wells and resulted in an additional 15 m of head decline in the production reservoir.

The delay between the pressure drop in the production reservoir in 1991 and the subsidence centered around the production wells in 1993 could

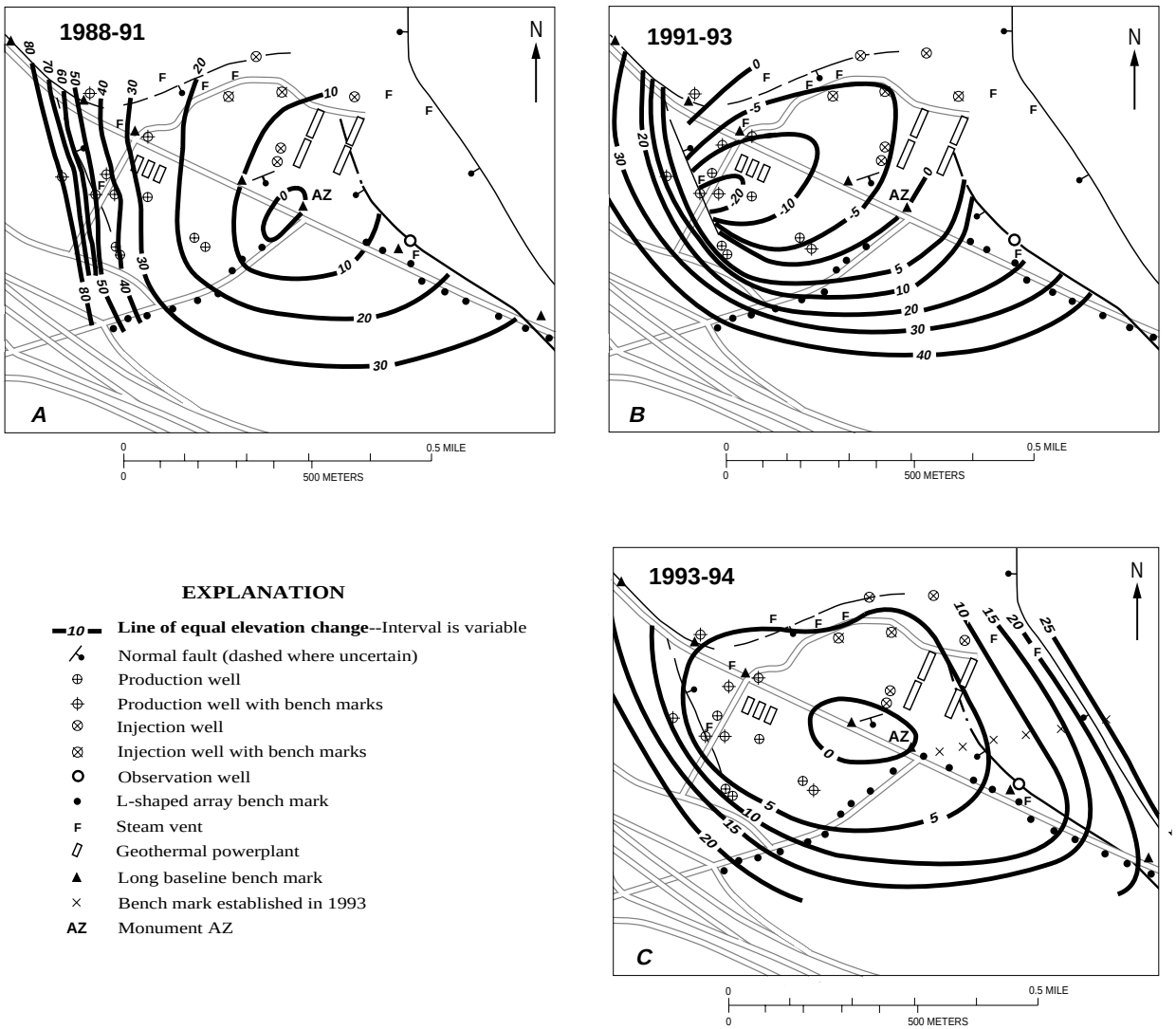

Figure 5. Land-surface elevation change, in millimeters, in the Casa Diablo geothermal well field. *A*, 1988–91. *B*, 1991–93. *C*, 1993–94. Modified from Sorey and others, 1995.

have been caused by thermal expansion of rocks above the production reservoir. A large increase in the volume of steam discharged from fumaroles and along faults was observed during 1991 and most of 1992. The increase in steam discharge was caused by boiling in the reservoir induced by the pressure drop. Thermal expansion was reversed when cold shallow ground water moved toward the pressure low at the production wells.

The data for 1994 show a shift in the area of maximum subsidence towards the center of the graben (fig. 5*C*). The greater degree of isolation between the injection and production reservoirs possibly allowed the pressure drop in the production reservoir to spread across the well field to include the central part of the graben. If very fine-grained materials compose the central part of the graben, the reduction in pore pressure would initiate a slow dewatering process that would

propagate from the production wells to the center of the graben. The changes in the location of maximum subsidence between 1993 and 1994 also could be related to changes in the production and injection rates of individual wells in the geothermal field.

REFERENCES CITED

Hill, D.P., Bailey, R.A., and Ryall, A.S., 1985, Active tectonic and magmatic processes beneath Long Valley Caldera, eastern California—An overview: American Geophysical Union, Journal of Geophysical Research, v. 90, no. B13, p. 11,111–11,129.

Langbein, J., 1989, Deformation of the Long Valley Caldera, eastern California, from mid-1983 to mid-1988: American Geophysical Union, Journal of Geophysical Research, v. 94, no. B4, p. 3,833–3,850.

Langbein, J., Hill, D.P., Parker, T.N., and Wilkinson, S.K., 1993, An episode of reinflation of the Long Valley Caldera, eastern California, 1989–1991: American Geophysical Union, Journal of Geophysical Research, v. 98, no. B9, p. 15,851–15,870.

Savage, J.C., Cockerham, R.S., Estrem, J.E., and Moore, L.R., 1987, Deformation near the Long Valley Caldera, eastern California, 1982–1986: American Geophysical Union, Journal of Geophysical Research, v. 92, no. B3, p. 2,721–2,746.

Sorey, M.L., Farrar, C.D., Marshall, G.A., and Howle, J.F., 1995, Effects of geothermal development on deformation in the Long Valley Caldera, eastern California, 1985–1994: American Geophysical Union, Journal of Geophysical Research v. 100, no. B7, p. 12,475–12,486.

Hydrogeologic Effects of Flooding in the Partially Collapsed Retsof Salt Mine, Livingston County, New York

By Dorothy H. Tepper, William M. Kappel, Todd S. Miller, *and* John H. Williams

The Retsof Salt Mine is in Livingston County, New York, about 25 mi (40 km) southwest of Rochester (fig. 1). This mine, which has been in operation for 110 years and is about 1,100 ft (335 m) below land surface, supplies road salt to 14 States in the Northeast. Retsof Salt Mine is the largest salt mine in the Western Hemisphere and includes an underground area that is roughly the size of Manhattan (6,500 acres or about 2,630 hectares). An underground room near the southern end of the mine near Cuylerville collapsed on March 12, 1994, and an adjacent room collapsed in early April. Two large, circular collapse features that are several hundred feet apart have developed at land surface above the two collapsed mine rooms. The northernmost feature, which is about 700 ft (213 m) in diameter, includes a central area about 200 ft (60 m) wide that has subsided about 20 to 30 ft (6 to 9 m). The southernmost feature, which is about 900 ft (274 m) in diameter, includes a central area that is about 700 ft (213 m) wide that has subsided about 70 ft (21 m). The subsidence in the collapse area has forced the closure of a section of State Route 20A as a result of the partial collapse of a New York State Department of Transportation bridge.

During the formation of these collapse features, hydraulic connections formed between aquifers and the mine that had been previously isolated from each other by confining units. These new connections have provided routes for rapid migration of ground water downward to the mine level. Since March 12, ground water draining from overlying aquifer systems has been progressively flooding the mine at inflow rates averaging about 18,000 gal/min (1,135 L/s). This aquifer drainage has caused inadequate water supplies in a number of local wells, and some wells actually have gone dry. The U.S. Geological Survey (USGS) has been working with the Livingston County Department of Health since March 1994 to provide technical expertise in dealing with this situation. A regional ground-water-level monitoring network has been established to observe the rate, magnitude, and extent of aquifer drainage related to the mine collapse. Data collected since the initial collapse show that water levels in some wells drilled in the flood-plain sediments and upland bedrock units are showing only expected seasonal changes. Significant water-level declines resulting from aquifer drainage into the mine have been observed in some wells completed in glacial deltaic deposits along the valley walls in an extensive basal sand-and-gravel aquifer in the Genesee Valley and in the uppermost bedrock near the collapse features (fig. 1). The basal sand-and-gravel aquifer and the thin water-bearing zone at the top of bedrock are hydraulically connected.

A conceptual model of the ground-water flow system has been developed on the basis of knowledge of the hydrogeology of similar valleys in central and western New York, borehole geophysical surveys of 18 wells drilled in and adjacent to the collapse features, and marine seismic-reflection profiling on the Genesee River. The complex ground-water flow system involves multiple aquifers in the glacial sediments and the bedrock. In June 1994, a team of specialists from the USGS examined the environmental effects of the partial collapse of the mine. The team compiled a list of options for further short-term and long-term studies to address the major issues of public safety, aquifer drainage, and subsidence. The USGS, the mining company, and the Livingston County Department of Health continue to monitor ground-water levels in the area, and the USGS is constructing a preliminary numerical model to assess the long-term effects of the partial mine collapse on the regional ground-water flow system.

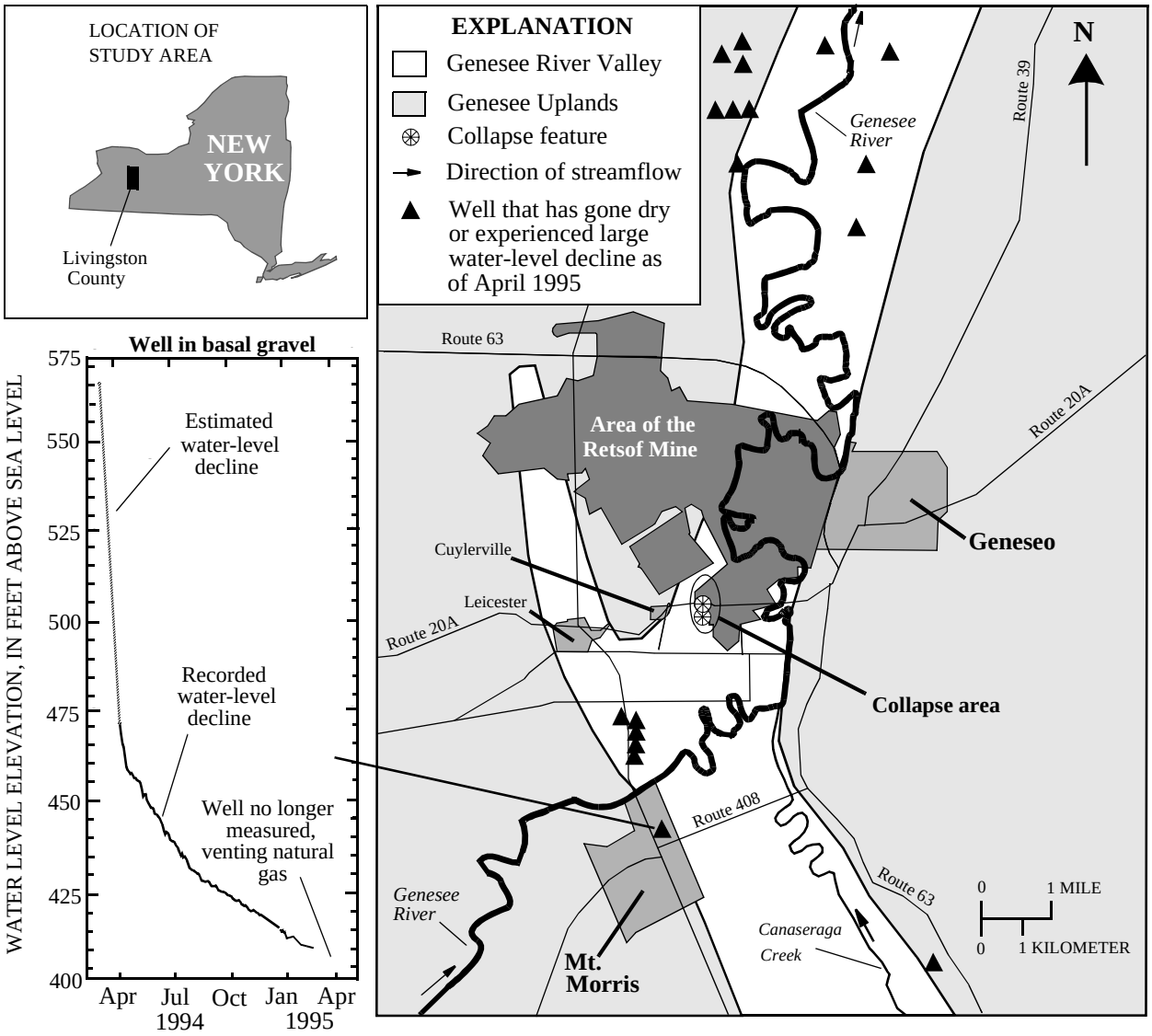

Figure 1. Location of Retsof Salt Mine, area of collapse, and hydrograph of water-level decline in a well 3.5 miles from the mine.